JAERI-M
90-123

CENTRAL MHD ACTIVITIES AND ROLE OF THE q=1 RATIONAL SURFACE FOR PELLET FUELLED JT-60 PLASMAS

August 1990

Yutaka KAMADA, Takahisa OZEKI, Masafumi AZUMI
Ryuji YOSHINO, Masayuki NAGAMI and Shigeru KONOSHIMA

日本原子力研究所
Japan Atomic Energy Research Institute

JAERI-M レポートは，日本原子力研究所が不定期に公刊している研究報告書です。
入手の問合わせは，日本原子力研究所技術情報部情報資料課（〒319-11茨城県那珂郡東海村）あて，お申しこしください。なお，このほかに財団法人原子力弘済会資料センター（〒319-11 茨城県那珂郡東海村日本原子力研究所内）で複写による実費頒布をおこなっております。

JAERI-M reports are issued irregularly.
Inquiries about availability of the reports should be addressed to Information Division Department of Technical Information, Japan Atomic Energy Research Institute, Tokai-mura, Naka-gun, Ibaraki-ken 319-11, Japan.

編集兼発行　日本原子力研究所
印　　刷　㈱高野高速印刷

JAERI-M 90-123

Central MHD Activities and Role of the q=1 Rational Surface for Pellet Fuelled JT-60 Plasmas

Yutaka KAMADA, Takahisa OZEKI, Masafumi AZUMI
Ryuji YOSHINO, Masayuki NAGAMI and Shigeru KONOSHIMA

Department of Large Tokamak Research
Naka Fusion Research Establishment
Japan Atomic Energy Research Institute
Naka-machi, Naka-gun, Ibaraki-ken

(Received July 9, 1990)

Improved energy confinement for the pellet fuelled plasmas on JT-60 is mainly due to the peaked density and pressure profiles inside the q=1 rational surface, where the confinement characteristics appear to be better than those in the outer (q>1) region. In the well-center-fuelled pellet injection discharges, the sawtooth activity can be suppressed completely during 0.4~1 sec or the frequency of sawteeth are reduced by up to one order of magnitude during 0.5~1.5 sec after the pellet injection. For high high-current low-q (Ip=2.5~3.1 MA; q(a)<3) discharges, reduction in the sawtooth frequency has a strong relationship with enhanced confinement and peakedness of the electron density profile. The contribution of the sawtooth activity to the global energy confinement increases systematically with decreasing q(a). At the sawtooth emerging after the pellet injection into high-Ip limiter discharges, only small amount of the central kinetic energy is released and the sawtooth dose not follow the fully reconnecting style. The release of the central kinetic energy and the existence of precursor and successor m=1 oscillations are discussed. The sawtooth crash tends to have more ideal-like characteristics for higher beta values and lower safety factors. The rotation velocity of the central plasma column after the pellet injection is also discussed with the frequencies of the m=1 oscillations. Just after the pellet injection, the plasma column starts to rotate in the ion-diamagnetic direction or the co-direction to the plasma current. At each sawtooth, the rotation frequency changes

suddenly to the ion-diamagnetic direction or the co- direction.

Keywords: Tokamak, Pellet Injection, Confinement, MHD, Sawtooth, β-value, Density, JT-60

ＪＴ－６０ペレット入射プラズマにおける中心MHD揺動とｑ＝１有理面の閉じ込め改善に対する役割

日本原子力研究所那珂研究所臨界プラズマ研究部
鎌田　裕・小関　隆久・安積　正史・永見　正幸
芳野　隆治・木島　滋

（１９９０年７月９日受理）

ＪＴ－６０のペレット入射実験における閉じ込め改善は，主にｑ＝１面内でピークした密度ないし圧力分布によって担われており，この領域はｑ＞１領域に比べて閉じ込め特性が良好に見える。良好な中心ペレット入射時にはsawtooth 振動は0.4～１秒間全く抑制されるか，あるいは0.5～1.5秒間にわたりその周期がガスパフ時に比べて最大１桁伸長する。高プラズマ電流低q 放電ではこのｓａｗｔｏｏｔｈ周期の伸長，閉じ込め改善度ないし電子密度のピーク度は強く関係し，ｓａｗｔｏｏｔｈ振動のグローバルな閉じ込めに対する寄与はq(a)の低下とともに系統的に増大する。高プラズマ電流のリミタ放電ではｓａｗｔｏｏｔｈ時に吐き出される中心熱エネルギーは小さく，ｓａｗｔｏｏｔｈが完全リコネクションモデルに従わないことを示し，このエネルギー吐き出し及びｍ＝１の前兆／後兆振動とベータ値の関係を議論する。ｓａｗｔｈｏｏｔｈ崩壊はベータ値が高い程，ｑ値が低い程理想モード的な性格を示す。さらに，ｍ＝１振動の周期に基づいたプラズマ回転についても議論を行なう。ペレット入射後には，プラズマコアはｉｏｎ－ｄｉａｍａｇｎｅｔｉｃ方向あるいはプラズマ電流に対し順平行方向に回転する。また各ｓａｗｔｏｏｔｈ崩壊により，プラズマ回転が同方向にシフトすることが示される。

那珂研究所：〒３１１－０１　茨城県那珂郡那珂町大字向山８０１－１

Contents

目　　次

1. INTRODUCTION

In JT-60, hydrogen pellets were injected into hydrogen discharges heated by OH, NB [1,2], LHRF [3] and/or ICRF [4]. Energy confinement time (τ_E) was enhanced up to 40% relative to usual gas fuelled discharges at the medium NB or NB+ICRF heating power of ~10~20MW for which the strongly peaked pressure profile was sustained within 0.5~1.0 sec after a series of pellet injection [1,2,5]. One of the interesting characteristics for the improvement is its strong dependence on the central magnetohydrodynamic (MHD) behavior, namely the sawtooth activity. Reduction in the sawtooth frequency has a strong relationship with enhanced confinement and peakedness of the electron density profile.

Pellet fuelling experiments on many tokamaks have been demonstrated its advantages of enhanced energy confinement. After pioneering studies on ISX tokamaks [6], the enhanced confinement characteristics due to the peaked density profile have been observed on medium sized tokamaks viz. ALCATOR-C [7], D-III [8], TFR [9],ASDEX [10], JFT-2M [11] etc. and large sized devices viz. TFTR[12] and JET[13]. In these previous works, the peaked density profile is strongly affected by sawteeth. However, there has not been reported explicitly that the q=1 surface is expected to play a particular role in the confinement properties for pellet injected discharges. This report presents the detailed behaviors of the central MHD activities, the sawtooth activity and the m=1 continuous oscillations, observed for the pellet fuelled JT-60 plasmas with which we can study the behavior of the MHD activities for a highly peaked pressure (or density) profile. The highest plasma pressure (ion + electron) in JT-60 pellet fuelled discharges have reached up to ~2 atm. The understandings of the sawtooth in such a pressure regime is required to design the next-step devices like ITER.

Although the study on the sawtooth activity has been one of the important aspects of the tokamak research since the first discovery in the ST tokamak [14], theoretical explanation for the sawtooth crash has not been completed [15,16]. Moreover, the observed structure of sawteeth exhibits complexity after the introduction of TFTR[17], JET[18] and JT-60[19] where the sawtooth can occur without observed precursor oscillations and the crash time is much faster than the conventional prediction. The main fields of the recent experimental works are i) to examine the feature of the sawteeth; the trigger mechanism of the sawtooth collapse or the relationship between the collapse and the m=1 continuous oscillations before and after the crash, precursor and successor oscillations, and displacement of the central hot core using the tomography technique [20~22] and ii) to examine the methodology of the sawtooth suppression with neutral beam heating (NBI) [23,24], ion cyclotron heating (ICH) [25], lower hybrid-current drive (LHCD) [26-29], electron cyclotron heating (ECH) [30,31] and pellet injection [1,7,12]. The main observation for the former aspect is that the sawtooth crash is an activity independent of the continuous m=1 mode [32,33] and central q value is not necessarily increased above unity

after the sawtooth crash [34]. In the latter aspect, the key parameter for the sawtooth suppression seems to be the beta value or pressure, including the high-energy ions [35,36] and electrons, as well as change in the current density profile. This paper concentrates on the role of the q=1, q being the safety factor, rational surface for the improvement in NB heated, pellet fuelled limiter discharges and shows the structure of the sawtooth and m=1 activities for these discharges which have highly peaked thermal pressure profiles inside the q=1 surface with peaked electron density and nearly flat electron temperature in the central region. With combining other studies treating the peaked pressure profile with peaked temperature and broad density profiles or with high energy particles, the total understandings of the general effects of the pressure on the sawtooth activity will be constructed. In this report the presentation is phenomenological. Due to the lack of the measurement of the central current density profiles, the precise feature of the stability for the internal modes is not discussed here.

The pellet injector produces 4 pellets (3mmΦ×2 and 4mmΦ×2) with velocities approaching 2.3km/sec [2,5]. The basic scenario of pellet injection, the plasma equilibrium configuration and diagnostic systems were presented in ref.[1] and the global confinement properties for high current (I_p~3.1MA) discharges will be reported in ref.[5]. In contrast to JET [13] where pellets were injected into sawtooth-free (q(0)>1) discharges, we injected the pellets into discharges with q(0)<1 and obtained the following characteristics.

This report is arranged as follows: Section 2 gives the role of the q=1 rational surface for the improved confinement produced by pellet injection. A brief review for previous works in JT-60 is also given in this section. In Section 3, the relationships among the sawtooth period, density peaking factor and the improved confinement are discussed. Section 4 presents the characteristics of saweeth and m=1 continuous oscillations after the pellet injection. Section 5 deals with change in the plasma rotation due to the pellet injection and following sawteeth crashes. In Sec 6, other topics of the MHD behavior are shown. Finally, in Sec.7, we summarize the conclusion. In Appendices, detailed time histories of soft-X ray signals for a typical discharge etc. are given.

2. ROLE OF THE q=1 SURFACE FOR IMPROVED CONFINEMENT

Figure 1 gives the relationship between the stored energy measured with a diamagnetic loop W^{DIA} and the absorbed power P_{abs} for NB heated limiter discharges with the plasma current I_p of 1.5, 2.1, 2.8 and 3.1MA. Data for pellet fuelled discharges are shown by closed symbols. The increase in W^{DIA} is up to 30%~40% as compared to the reference lines of gas fuelled scalings [1,2,5]. For each I_p and P_{abs}, only the pellet cases having the highest improvement are plotted. The pellet data with smaller improvement scatter between the closed and open (gas fuelled data) symbols. It must be noted that the incremental confinement time τ_E^{inc}

after the sawtooth crash [34]. In the latter aspect, the key parameter for the sawtooth suppression seems to be the beta value or pressure, including the high-energy ions [35,36] and electrons, as well as change in the current density profile. This paper concentrates on the role of the q=1, q being the safety factor, rational surface for the improvement in NB heated, pellet fuelled limiter discharges and shows the structure of the sawtooth and m=1 activities for these discharges which have highly peaked thermal pressure profiles inside the q=1 surface with peaked electron density and nearly flat electron temperature in the central region. With combining other studies treating the peaked pressure profile with peaked temperature and broad density profiles or with high energy particles, the total understandings of the general effects of the pressure on the sawtooth activity will be constructed. In this report the presentation is phenomenological. Due to the lack of the measurement of the central current density profiles, the precise feature of the stability for the internal modes is not discussed here.

The pellet injector produces 4 pellets (3mmϕ×2 and 4mmϕ×2) with velocities approaching 2.3km/sec [2,5]. The basic scenario of pellet injection, the plasma equilibrium configuration and diagnostic systems were presented in ref.[1] and the global confinement properties for high current (I_p~3.1MA) discharges will be reported in ref.[5]. In contrast to JET [13] where pellets were injected into sawtooth-free (q(0)>1) discharges, we injected the pellets into discharges with q(0)<1 and obtained the following characteristics.

This report is arranged as follows: Section 2 gives the role of the q=1 rational surface for the improved confinement produced by pellet injection. A brief review for previous works in JT-60 is also given in this section. In Section 3, the relationships among the sawtooth period, density peaking factor and the improved confinement are discussed. Section 4 presents the characteristics of saweeth and m=1 continuous oscillations after the pellet injection. Section 5 deals with change in the plasma rotation due to the pellet injection and following sawteeth crashes. In Sec 6, other topics of the MHD behavior are shown. Finally, in Sec.7, we summarize the conclusion. In Appendices, detailed time histories of soft-X ray signals for a typical discharge etc. are given.

2. ROLE OF THE q=1 SURFACE FOR IMPROVED CONFINEMENT

Figure 1 gives the relationship between the stored energy measured with a diamagnetic loop W^{DIA} and the absorbed power P_{abs} for NB heated limiter discharges with the plasma current I_p of 1.5, 2.1, 2.8 and 3.1MA. Data for pellet fuelled discharges are shown by closed symbols. The increase in W^{DIA} is up to 30%~40% as compared to the reference lines of gas fuelled scalings [1,2,5]. For each I_p and P_{abs}, only the pellet cases having the highest improvement are plotted. The pellet data with smaller improvement scatter between the closed and open (gas fuelled data) symbols. It must be noted that the incremental confinement time τ_E^{inc}

for pellet fuelled discharges is almost equal to τ_E^{inc} for gas fuelled discharges. In other words, the enhanced stored energy (ΔW) is almost constant and independent of P_{abs}. This is because the improvement due to the pellet injection is mainly based on the enhanced stored energy within the q=1 rational surface r_s, and the measured maximum pressure gradient and total pressure inside r_s seem to be consistent with the critical values for the ideal ballooning and the internal kink instabilities [37]. One of the main objectives of this report is to clarify these limitation with experimental observations.

Figure 2 shows electron pressure p_e (electron density n_e × electron temperature T_e) profiles for pellet fuelled discharges (I_p=3.1, 2.8, 2.1 and 1.5MA, safety factors at the plasma surface q(a)=2.3, 2.3, 3.3 and 4.2), gas fuelled reference data (I_p=2.8 and 2.1MA) and positions of the q=1 rational surfaces (r_s) determined with the sawtooth inversion radii. The electron pressure profiles were constructed with combinations of Thomson scattering, ECE and soft-X ray emission (SX) data. The availability of SX measurements for the electron pressure profile was discussed in Appendix-A. About 50~70% of the enhancement in the stored energy ΔW is based on the peaked portion of the pressure profile inside r_s.

Figure 3 shows $n_e(r)$ and $T_e(r)$ measured at 0.8 sec after the pellet injection for a 3.1MA limiter discharge (Bt=4.8T, q(a)=2.3). It can be understood that the peaking of the electron pressure ($n_e \times T_e$) profile is due to the peaked electron density profile. Such peaked n_e profiles can be obtained when the sawtooth activity is suppressed. The figure also shows time evolutions of soft-X ray intensity for two chords of r=0 and 42 cm. In this case, the sawtooth repetition time in the pre-pellet portion is 80~100 msec and the sawtooth activity is suppressed completely during ~0.8sec after the pellet injection.

We scanned I_p (0.5~3.1MA) and the toroidal magnetic field B_t (3.5~4.8T) to survey the dependence of the width of the peaked portion of the electron pressure (r_p) on q(a) (Fig.4). The solid line in Fig.4(a) indicating r_s for gas fuelled discharges is written by r_s=a/q(a) (a is the plasma minor radius, ~0.9m for limiter discharges). Figure 4(b) shows the soft-X ray emission profiles (~p_e^2) normalized by the central values for three cases with different q(a) and gives the definition of r_p. The width (r_p) increases linearly with 1/q(a) and the values agree systematically with the q=1 surface (r_p=r_s). In well-center-fuelled discharges, the sawtooth activity can be suppressed completely during 0.4~1 sec after the pellet injection and then a large sawtooth recovers or the frequency of sawteeth are reduced during 0.5~1.5 sec after the pellet injection. These sawteeth have the same inversion radii of r_s~a/q(a). After the pellet injection, large m=1 continuous oscillations are observed during the sawtooth-free phase, structures of these m=1 modes indicate that r_p ~ a/q(a). Therefore it is concluded that the pressure profile produced by the pellet injection peaks inside the q=1 surface. Since the electron temperature in the central region is cooled adiabatically after the pellet injection, the central current density profile,

therefore the magnetic shear, can be modified because of the ohmic dissipation and the penetration of the poloidal magnetic field B_p. For the NB-heated JT-60 plasmas, a calculation of the current re-distribution shows that the safety factor at the plasma center dose not change drastically after the pellet injection because the re-heating time is short enough to keep the central q below unity [38]. In such the scan of q(a), of particular interest is the improvement by pellets at low-q. For the divertor configuration, the degradation of the energy confinement time in the $q_{eff}<3$ region recovers to the level for the $q_{eff}>3$ region due to the sawtooth suppression [1]. On the other hand, for limiter configuration, the confinement dose not degrade in the law-q region for gas fuelled discharges [39]. There is no marked qualitative difference observed in the time evolution of the pellet injected limiter discharges in a wide range of the safety factor.

After the injection for most of the discharges, the electron pressure rises gradually inside r_s until a sawtooth reappears. However, in well-center fuelled and NB heated discharges, the pressure gradient saturates at a certain value before the first sawtooth reappears [1]. Figure 5 gives the time evolution for the profiles of Abel inverted SX emission (Fig.5(a)) and those of electron pressure gradient estimated with SX signals (Fig.5(b)) for a 2.1MA limiter discharge heated by NB (P_{abs}=13MW). Pellets were injected at t=6.0sec. The SX-profile peaks strongly inside r_s. During the pressure peaking phase, the p(r) profile evolves only inside r_s and the position is kept almost constant (r_s~28cm). At first, the saturation occurs locally at the outer portion inside r_s, then the pressure gradient reaches the limiting value in the inner region. The saturated value scales roughly with B_t^2 and reaches the critical value determined by the high-n (n being the toroidal mode number) ideal ballooning instability [2,37]. In Figure 5 (b), the calculated balloon-limits are drawn for two cases with assumed q(0) of 0.98 and 0.90. In the former case, the pressure gradient reaches the balloon-limit at r<23cm. When the sawtooth activity is not suppressed completely, the pressure gradient dose not reach the balloon limit and the central pressure is released gradually due to the sawteeth crashes.

The highly peaked pressure profile can be achieved only when the pellet penetration is deep enough and the peakedness is a strong function of the penetration. Figure 6 shows the dependence of W^{DIA} on the penetration depth from the axis measured with the pellet monitor for 2.1 and 2.5 MA discharges. For both sets, four pellet-injected and a gas-puffed shots with the same P_{abs} of 10MW are included. The stored energy increases drastically when pellets penetrate into the core region (r<30cm ~ r_s), otherwise the stored energy of the pellet shots shows little enhancement relative to the gas fuelled cases. In Fig.6 time evolutions of the SX profiles for the four 2.1 MA discharges are also given. The peaked SX profile corresponding to the distinct improvement in W^{DIA} can be produced only when the pellets penetrate deeply into the plasma.

Figure 7 shows $n_e(r)$ for 0.02 and 0.4 sec after the pellet injection and that for the gas fuelling (before the injection). At 0.02 sec after the injection, n_e profile is broad. At 0.4 sec after

the pellets, the n_e profile peaks inside r_s. Therefore, the particle confinement inside r_s seems to be better than that in the outer region. The figure also suggests the inward pinch of the plasma particles. In our present status, however, conclusive transport analyses separating the particle diffusivity and the inward pinch velocity have not been made. The details for the transport characteristics will be discussed elsewhere [5]. Plasma equilibrium may be modified in the core region of $r<r_s$ and the confinement property is improved. The evidence, however, has not been observed so far.

3. SAWTOOTH ACTIVITY AND IMPROVED CONFINEMENT

The peakedness of electron density profile depends strongly on the penetration depth of the pellets. When the pellet penetrates inside or close to r_s, the sawtooth activity can be suppressed completely during 0.4-1.0 sec or the frequency of sawtooth are reduced by up to one order of magnitude. Since the sawtooth activity flattens the peaked pressure profile, the occurrence of the mode has a direct influence on the global confinement especially for low-q (q(a)<3) discharges.

3.1 Limiter Discharges

Figure 8 shows the time evolutions of stored energy (W^{DIA}) and the SX emission for the central and r=42cm chords for a 2.8MA limiter discharge (q(a)=2.35). In this case, the sawtooth activity is not suppressed completely after the pellet injection. For the high-current (Ip=2.5~3.1MA; q(a)<3) limiter discharges, only small amount of the central kinetic energy is released at the sawtooth, and the sawtooth activity dose not follow the fully reconnecting style (see Sec.4). The observation gives the fact that the q=1 rational surface survives during the sawtooth crash and the central kinetic energy is not released completely due to the crash.

Figure 9 gives the relationships among ΔW (improvement in the stored energy compared to the gas fuelled scaling), peaking factors of the n_e profiles (F_{np}) and the averaged sawteeth periods (τ_{st}) for I_p/B_t=2.8MA/4.5T and 3.1MA/4.8T limiter discharges with P_{abs} of 16~19MW and q(a)~2.35. ΔW corresponds mainly to the enhanced stored energy associated with the plasma core. ΔW is taken at the time of Thomson scattering measurement (t_{Thom}) which is around the time when the stored energy becomes its maximum value (t_{Wmax}). The contribution of dW/dt to the calculation of the energy confinement time is negligible and the energy confinement time τ_E in this report is defined by W^{DIA}/P_{abs}. The value 'τ_{st}' is the sawtooth period averaged from the injection time to t_{Thom}. As mentioned before the whole central stored energy is not released at one sawtooth crash, therefore, the stored energy can increase (in time) even after a sawtooth. In these conditions, the averaged sawtooth period is a good measure to indicate the central confinement degradation due to the sawtooth activity. The peaking factor of n_e (F_{np})

the pellets, the n_e profile peaks inside r_s. Therefore, the particle confinement inside r_s seems to be better than that in the outer region. The figure also suggests the inward pinch of the plasma particles. In our present status, however, conclusive transport analyses separating the particle diffusivity and the inward pinch velocity have not been made. The details for the transport characteristics will be discussed elsewhere [5]. Plasma equilibrium may be modified in the core region of $r<r_s$ and the confinement property is improved. The evidence, however, has not been observed so far.

3. SAWTOOTH ACTIVITY AND IMPROVED CONFINEMENT

The peakedness of electron density profile depends strongly on the penetration depth of the pellets. When the pellet penetrates inside or close to r_s, the sawtooth activity can be suppressed completely during 0.4-1.0 sec or the frequency of sawtooth are reduced by up to one order of magnitude. Since the sawtooth activity flattens the peaked pressure profile, the occurrence of the mode has a direct influence on the global confinement especially for low-q (q(a)<3) discharges.

3.1 Limiter Discharges

Figure 8 shows the time evolutions of stored energy (W^{DIA}) and the SX emission for the central and r=42cm chords for a 2.8MA limiter discharge (q(a)=2.35). In this case, the sawtooth activity is not suppressed completely after the pellet injection. For the high-current (Ip=2.5~3.1MA; q(a)<3) limiter discharges, only small amount of the central kinetic energy is released at the sawtooth, and the sawtooth activity dose not follow the fully reconnecting style (see Sec.4). The observation gives the fact that the q=1 rational surface survives during the sawtooth crash and the central kinetic energy is not released completely due to the crash.

Figure 9 gives the relationships among ΔW (improvement in the stored energy compared to the gas fuelled scaling), peaking factors of the n_e profiles (F_{np}) and the averaged sawteeth periods (τ_{st}) for I_p/B_t=2.8MA/4.5T and 3.1MA/4.8T limiter discharges with P_{abs} of 16~19MW and q(a)~2.35. ΔW corresponds mainly to the enhanced stored energy associated with the plasma core. ΔW is taken at the time of Thomson scattering measurement (t_{Thom}) which is around the time when the stored energy becomes its maximum value (t_{Wmax}). The contribution of dW/dt to the calculation of the energy confinement time is negligible and the energy confinement time τ_E in this report is defined by W^{DIA}/P_{abs}. The value 'τ_{st}' is the sawtooth period averaged from the injection time to t_{Thom}. As mentioned before the whole central stored energy is not released at one sawtooth crash, therefore, the stored energy can increase (in time) even after a sawtooth. In these conditions, the averaged sawtooth period is a good measure to indicate the central confinement degradation due to the sawtooth activity. The peaking factor of n_e (F_{np})

is defined by $n_e(0)/<n_e>$ (central value / volume averaged value). In case of Fig.8, these data were taken at t_{Thom}=6.4 sec and ΔW=0.3MJ, F_{np}=2.2 and τ_{st}=0.2sec. For usual gas fuelled discharges with the same operation parameters with Fig.9 have F_{np}=1.2~1.3 and τ_{st}~0.07~0.08sec. In Fig.9, differences in the density peaking are due to differences in pellet penetration depth which can be changed by pellet numbers, time interval of succeeding pellets, n_e and P_{abs} for the target plasmas. Figure 9(a) indicates that ΔW increases linearly with F_{np}. Figures 9(b) and (c) show dependences of F_{np} and ΔW on τ_{st}, respectively. F_{np} (and ΔW) increases with τ_{st} for τ_{st}<0.2 sec, and saturates for τ_{st}>0.2sec. At this saturation point, the ratio of τ_{st} for pellet injected discharges to the sawtooth period for gas fuelled discharges ,τ_{st}(pellet)/τ_{st}(gas puff), is ~2.5~3.

In Fig.10(a), the sawtooth period τ_{st} is normalized by τ_E and the saturation occurs at τ_{st}~1.4τ_E and further improvement cannot be obtained for τ_{st}>1.4τ_E. Figure 10(b) corresponds to the data with I_p=2.1MA (q(a)=3.3). In this case, the saturation occurs at τ_{st}/τ_E ~2.5 and the level is considered to be limited by the ballooning instability. Figure 10(c) gives the relationship between q(a) and τ_{st}/τ_E at the saturation point, $(\tau_{st}/\tau_E)_{strt}$, obtained in some data sets with different I_p. The contribution of the sawtooth activity on the global confinement becomes larger for lower q(a) discharges. For the two cases of q(a)=2.35 and 2.8 in Fig.10(c), the plasma dose not reach the balloon-limit at the saturation point and the saturation is determined by the transport properties independent of the MHD modes considered so far. While, in the other cases of q(a)=3.3 and 4.2, the saturation occurs due to the balloon-limit. The values of $(\tau_{st}/\tau_E)_{strt}$ for the two cases could be higher than the obtained values, if the plasma had not reach the balloon-limit.

3.2 Lower-X point Discharges

For the lower-X point discharges, the reduction in the sawtooth frequency has remarkable effects on the improved confinement in the q_{eff}<3 regime. Figures 11, 12 and 13 show the comparison of plasma parameters among gas fuelled (E8009), two-pellet (E8005) and tree-pellet injected (E8007) 1.8MA lower X-point discharges at the same P_{abs} of 9.5MW. In Fig.11, sets of traces for the three discharges are presented. For E8007, the line density averaged at r=0.7a increases immediately by $6\times10^{19}m^{-3}$, then decays slowly to the gas-fuelled level and the central electron temperature, $T_e(0)$, measured by ECE emission drops as the discharge is diluted by cold particles from the pellet, then, recovers with a time scale similar to the decay of $\bar{n}_e$. The stored energy for E8007 takes the maximum value at t=6.2 sec when $T_e(0)$ almost recovers to its initial value and decays simultaneously with the onset of a large sawtooth (shown later in Fig. 13). For E8005, $\bar{n}_e$(r=0.7a) just after the pellet injection is higher than that for E8007, however decays faster. This means the pellet does not penetrate deeply into the core region. Figure12 shows

profiles of n_e and T_e for the three discharges measured at t=6.2sec (0.4 sec after the pellet injection) with the Thomson scattering system. The T_e profiles for E8007 and E8005 have almost the same values with that for E8009, while $n_e(r)$ for the pellet discharges are kept much higher than that for the gas fuelled shot especially in the core region. Therefore the increase in the stored energy is concluded to depend mainly on the increased density. Figure 13 presents signal intensities of the soft-X ray emitted from the core region ; (a) and (b) show time evolutions of spatial distribution and those for the 4 chords near the magnetic axis, respectively.The SX profile for E8007 peaks strongly in a region inside Ch.10 for E8007. In turn, for E8005, the profile is flat in this region. For E8007 a small sawtooth is observed at t=6.04 sec, for E8005 repeating sawteeth occur from t=6.0 sec. Their inversion radii correspond to the position of the Ch.10. The stored energy of E8005 (Fig.11) saturates simultaneously with the onset of the first sawtooth at t=6.0 sec, and that of E8007 happens to decrease at t=6.2 sec also with the onset of the large sawtooth. From these observations, the SX profiles strongly peaked inside the sawtooth inversion radii (r_s) after the pellet injection are the key features of improved confinement characteristics of NB heated discharges. The energy confinement time τ_E for the pellet and gas fuelled discharges with B_t=4.5T and P_{abs}=8~12MW are plotted in Fig.14 as a function of the plasma current I_p. For the gas fuelled lower-x point discharges, the increase in τ_E with I_p is degraded at $q_{eff}<3$. While, for the pellet discharges, τ_E increases linearly with I_p at $q_{eff}<3$ and the improvement by the pellet injection is distinct in the low-q regime (I_p=1.8MA), this seems to be due to suppression of the sawtooth activity.

3.3 Discussion

In Fig.10, basically, the saturation may occur at $\tau_{st} \sim \tau_E(q=1)$, the energy confinement time representing the transport property across r_s. Therefore Fig.10(c) implies the relationship between the energy confinement at r=a and r=r_s. In the pellet injection experiments, the increase in the energy confinement time, density peaking and sawtooth suppression are linked closely. Therefore, with only the pellet injection experiments, we cannot conclude precisely whether the q<1 region has a favorable energy confinement characteristics universally or not. It can be observed that the particle confinement at q<1 region is better than that outside the q=1 surface with time evolutions of n_e-profiles and SX-profiles. If the particle confinement is good in this region, the density profile peaks in this region after the direct central fuelling of the pellet injection. The enhanced energy confinement may be the result of the density peaking and may not be due directly to the inherent small thermal diffusivity in this region. Such a speculation can be examined with comparisons of sawtooth suppression experiment without the density peaking viz. ICRF, LHRF or ECRF experiments.

4. CHARACTERISTICS OF SAWTEETH AND m=1 OSCILLATIONS

4.1 General Behavior

After the pellet injection for most of the discharges, the electron pressure rises gradually inside r_s until a sawtooth reappears. In well-center fuelled and NB heated discharges, the pressure gradient saturates at a certain value before the sawtooth. The pressure gradient of the discharges is considered to reach the marginal value for the infinite-n ballooning mode locally inside r_s. After reaching the marginal value in a magnetic surface, the marginally stable region spreads toward the axis. The total pressure inside r_s (or the poloidal beta within r_s, β_{p1}) has not reached the ideal ballooning limit optimized for all position inside r_s. The analysis with ERATO-code shows that the attained maximum β_{p1} is consistent with the internal n=1 kink mode beta limit [37]. This section studies the observed characteristics of sawteeth and m=1 oscillations. With deepening of the pellet penetration and peaking of the electron pressure profile, the following tendency of the central MHD behavior is observed;

i) Sawtooth period increases. Amplitude of the m=1 continuous oscillation and number of sawtooth with post-cursor oscillation increase.

ii) Sawtooth activity is suppressed for a long time (<1 sec) and the enhanced m=1 mode continues.

iii) Both sawteeth and m=1 modes are suppressed completely within ~1~1.5 sec.

Even in the case iii), the q(0) is considered to be below unity [1,2 and Sec. 1.3].

4.2 Sawteeth for the low-Ip lower-X point discharges

Figure 15 shows that the degradation in W^{DIA} occurs simultaneously with the onset of a sawtooth and the strongly peaked SX-profile is broadened at each sawtooth crash. For lower X-point discharges, the sudden decrease in W^{DIA} is usually observed at the first large sawtooth emerging after the pellet injection. Fig.15(a) compares traces of W^{DIA} for a pellet fuelled (E7994) and a gas fuelled (E8002) 1.5MA lower-X point discharges with the same NB power of 3.5MW. From t~6.21s, W^{DIA} in the pellet case decreases rapidly to the gas fuelled level. Figure 15(b) shows the time traces of SX emission rate for two chords seeing the center and r~2/3a for E7994. After the pellet injection, small sawteeth are observed within 0.4 sec. These sawteeth are characterized as partial collapses. After then no sawtooth but a large continuous m=1 mode is activated and W^{DIA} decreases gradually until t=6.21s. The first and the second large sawteeth occur at t=6.21s and t=6.29s, respectively. At each crash the peaked portion of the SX profile at $r \lesssim r_s$ (Ch.9~Ch.10) is drastically flattened (Fig.15(c)) and W^{DIA} happens to decrease. In Figs.16(a) and (b), evolutions of the SX-signals around the first large sawtooth crash are shown. For this crash, only the pre-cursor m=1 oscillation is observed and the m=1

structure disappears after the crash (Fig.16(a)). The centrally peaked portion of the SX-profile is released outward within 150 μsec (Fig.16(b)) and the produced profile is almost flat inside the mixing radius. This observation dose not contradict the fully reconnecting, or flattening, style of the sawtooth [22, 40]. For lower-X point discharges, most of the sawteeth show the similar feature even the pellet penetration is deep.

4.3 Sawteeth for the High-Ip Limiter discharges

For the high-current (Ip=2.5~3.1MA; q(a)<3) limiter discharges with deep penetration of pellets, only small amount of the central kinetic energy is released at the sawtooth, and the sawtooth activity dose not follow the fully reconnecting style [41]. Figure 17 shows time evolutions of W^{DIA}, $n_e l$ (r~0.5m), soft-X ray intensity (central chord) for a pellet fuelled 3.1MA limiter discharge (q(a)=2.3). Pellets were injected at t~6.0 sec. At the first and the second sawteeth at t=6.82 sec and 7.05 sec, the total stored energy is not affected by the sawteeth crashes. This observation gives a marked contrast to Figs.11 and 15 and suggests that a large amount the energy confined inside the q=1 surface is not released. This section discusses the behavior of sawteeth for the pellet fuelled high-current limiter discharges.

Figure 18 compares the time histories of the SX-signals (chords at r=0, r=42 and r=56cm) and the electron density profiles measured with the Thomson scattering system for four discharges of pellet injection with q_a~2.3 (I_p/B_t=2.8MA/4.5T and 3.1MA/4.8T). What is different among these discharges is the pellet penetration condition; the pellet penetration depth becomes deeper from the top (Fig.18(a)) to the bottom (Fig.18(d)) column of the figure. The ratio of the SX-intensity of the central chord between just before and just after the injection is a good measure for the pellet penetration. The values are (a)73.1%, (b)40.2%, (c)22.7% and (d)21.4% for thses four discharges. The poloidal β-values determined inside r_s ($\beta_p{}^1$) [42] for discharges in Fig.18 are (a) 0.07, (b) 0.22, (c) 0.24 and (d) 0.35. The error of the calculated value of $\beta_p{}^1$ is estimated to be 0.05. With deepening of the pellet penetration , the electron density peaking factor and $\beta_p{}^1$ increase, and the following tendency of the central MHD behavior is observed;

i) Sawtooth period increases. Amplitude of the m=1 continuous oscillation and number of sawtooth with post-cursor oscillation increase.

ii) Sawtooth activity is suppressed for a long time (<1 sec) and the enhanced m=1 mode continues.

iii) Both sawteeth and m=1 modes are suppressed completely within ~1~1.5 sec.

For the shallowest penetration in Fig.18(a), the sawtooth period becomes short after the injection. This may be because the density peaking factor for E10248 is comparable to that for the gas fuelled discharges and the averaged electron temperature is lower than that for gas fuelled discharges.

The important change of the sawtooth characteristics is the change of the crash mechanism. In Fig.19, the SX-profiles just before (t=7.3971s) and after (t=7.3974s) a sawtooth crash are shown in a shallow penetration case, where the central portion of the SX-profile at r<30cm is almost flattened. This crash is observed to have the same feature with that shown in Fig.16 for the low-current lower-X point discharge. Generally, for higher-q and lower-$\beta_p{}^1$ discharges in JT-60, the sawtooth crash behaves like this. Such sawteeth often have precursor m=1 oscillation and very small or no postcursor oscillation. In contrast, for lower-q and higher-$\beta_p{}^1$ discharges, the sawtooth crash tends to follow incomplete reconnection and the postcursor oscillation becomes larger.

Figures 20, 21 and 22 give the behavior of SX emission for the 2.8MA (q(a)=2.34) discharge (E10324; the same discharge with Fig.18(b), the time trace of W^{DIA} was shown in Fig.8.) where the sawtooth activity is not suppressed completely. The high frequency oscillation in Fig.20(b) is the (m,n)=(1,1) oscillation and the mode appears continuously before (precursor) and after (postcursor) the sawtooth crash. The similar behavior of the m=1 continuous mode was also observed on JET [43]. Figure 20(c) shows the evolution of the profile of $\widetilde{SX}/\overline{SX}$ (fluctuating part/averaged part) for the m=1 oscillation during the sawtooth period. The peak radius of the continuous mode, $r_{m=1}$, is small (~14cm) after the sawtooth crash. The radius increases gradually and reaches 35cm (~a/q(a)) before the next crash. The time evolution of $r_{m=1}$ is given in Fig.20(d). After the sawtooth crash at t=6.4115sec, $r_{m=1}$ moves inward with the time scale of ~10msec which is much longer than the sawtooth crash time (~400μsec). These observations give the fact that the q=1 rational surface survives during the sawtooth crash and the central kinetic energy is not released completely due to the crash. The SX-emission profiles just before and after the sawtooth at t=6.4115sec are shown in Fig.21. Figures 21(a) and (b) gives the SX-profiles detected by the lower and upper PIN-diode arrays. The figures show that the central core shifts (m=1 displacement) and is not flattened completely. Figure 22 indicates the time histories of crash times and the mixing radii. After the pellets injected at t=6.0sec, the crash time increases. The sawtooth crash time is typically about 300~600μsec, which is longer than that (~100 ~200 μsec) for gas fuelled discharges. While, the mixing radius dose not change. This observation means that the global current distribution after the pellet injection is similar to that in the gas fuelled portion of the discharge and the change in the crash time is due to some reasons other than the change of current distribution.

In Fig.18(c), amplitude of the successor m=1 oscillation is larger than the amplitude of the crash. For the discharge, Fig. 23 shows the time evolution of the central SX-signal and the SX-profiles before and after the sawtooth crash. The timings of t=7.2988s and t=7.3043s are chosen to have the same phase of the m=1 oscillations. It can be observed that only the central portion of the SX-profile is decreased and the m=1 peak survives almost unchanged or some

amount of the SX-sorce seems to be transported from the central region to the island region. This observation clearly gives that the sawtooth crash can be independent of the m=1 continuous oscillation.

Figure 24 shows time evolutions of SX-signals for E10814 (given in Figs.17 and 18(d)) from t=6.8s to t=7.4s. The first and the second sawteeth after the pellet injection (t=6.0s) occur at t~6.87s and t~7.01s, respectively, and the total stored energy dose not decrease due to these sawteeth (see fig.17). (The decrease in W^{DIA} occurs slowly after t=7.03sec; see Fig.33.) In Fig.24, after the first sawtooth crash, the plasma becomes sawtoothing and continuous m=1 oscillations are observed around the crashes. The first crash has only the precursor oscillations and the second (7.01 sec) has both precursor and postcursor oscillations. The third crash has only the postcursors. Due to these obsevations, it seems to be difficult to understand the sawtooth crash only based on the discussion of m=1 behavior around the crash.

Figure 25(a) gives a gradual shift (m=1) of the plasma core before the second sawtooth from t=7.005s to 7.009s. With this observation of the m=1 displacement, the position of the q=1 surface can be identified at r~35cm. In Fig.25(b), the quick change in SX-profile due to the second sawtooth crash is presented. The central core shifts within the crash time of ~400μsec (from t=7.0092 to t=7.0096s), however almost all of the central SX-source inside the q=1 surface (r<35cm) is conserved and the released energy is small.

Figure 26 shows another example where the sawtooth activity is suppressed within ~1sec after the pellet injection. The small oscillations observed at t=6.5~6.8sec are partial sawteeth originated at r~0.1m during which the central SX emission remains almost unchanged and the release of the central energy is small. The appearance of the partial crash implies the q-profile in the core region is flat. In this particular discharge, the plasma core dose not rotate in the decay phase (t=7.2~7.7sec) of the central SX emission. Figure 26(b) indicates the time history for the contour lines of SX emission rate in the central region (r<50cm) from t=7.2 to 7.37 sec. The position of the q=1 surface is ~35cm. The hot and dense core shifts following the m=1 displacement, but behaves as a rigid body during the sawteeth (crash time~300μsec). The released kinetic energy is also small for the sawteeth. Figure 26(c) shows two profiles of the SX emission for t=7.3344sec (just before the crash) and 7.3347sec (just after the crash) and a plasma displacement in the radial direction estimated simply with the two SX-profiles. The shape of the displacement seems to be similar to that for the conventional ideal m=1 mode [44] rather than that for the quasi-interchange mode [41].

4.4 Discussion

In Fig.20, the central electron density before (t=5.9sec) and after (t=6.4sec) the injection are 8 and $24\times10^{19}m^{-3}$ and, therefore, the Alfven transit time after the pellet injection is about 1.7

times longer than that for the gas fuelled portion. If the sawtooth crash is an ideal instability, the increased crash time may be explained by the change in the Alfven time. On the other hand, the magnetic Reynolds number (S) for pellet discharges is about 1/10 ~1/20 of that for gas fuelled discharges. If the sawtooth is due to the m=1 resistive instability and the q-profile for pellet fuelled discharges is similar to that for the gas-fuelled discharges (see Fig.22(b), the growth rate have to increase because of the reduction of S. Experimentally, the sawtooth crash time increases. The observation may mean the sawtooth appeared after the injection is not the resistive mode. For pellet fuelled discharges, the sawtooth crash time tens to increase with increase in line averaged electron density. This tendency may be explained with change in the Alfven time if the sawtooth is triggered by the ideal kink mode.

The reason of the enhanced sawtooth period has not been identified. If the sawtooth period can be described mainly with the resistive diffusion time in the central region, the period for the pellet discharges must be shorter than that for the gas-fuelled discharges, because, generally, the central electron temperature for the pellet discharges are lower than that of the gas-fuelled discharges. The increased sawtooth frequency in Fig.18(a) after the pellet injection can be explained with this scenario. On the other hand, for peaked density (or pressure) profiles the sawtooth period cannot be explained only with the resistive diffusion of the plasma current.

Conclusive results, however, for the reasons of the enhanced sawtooth period and the mechanisms of the sawtooth crash (ideal or resistive) cannot be presented because we do not have the measured data of local shear around the rational surface. The experimental observations are : With increasing $\beta_p{}^1$ or the density gradient in the core region, the sawtooth period increases, the release of the central kinetic energy due to the sawtooth decreases and the sawtooth changes its characteristics from resistive (or reconnecting) type to ideal (non-reconnecting) type.

5. ROTATION OF THE PLASMA CORE

Direction of the m=1 mode rotation on the poloidal cross section is shown in Fig.24. In this discharge, the mode rotation changes the direction during the sawtooth ramping phases (t~7.22, 7.33sec) and at crashes (t~7.265, 7.355sec). From t=7.2 to 7.3s in Fig.24, the m=1 frequency is increased after the sawtooth crash. On the other hand, in Fig. 27, which shows a time history of m=1 mode before and after the sawtooth for a pellet injected Ip=2.8MA discharge (E8985), the m=1 frequency is decreased due tho the sawtooth crash. To understand the change in m=1 frequency during the ramping phase of sawteeth and after the sawtooth crashes, we examined the following analyses.

The frequency and the direction of the m=1 mode change with the balance of co- and counter-injected NBI powers (P_{co} and P_{cntr}) [45]. Figure 28 gives the relationship between the mode

times longer than that for the gas fuelled portion. If the sawtooth crash is an ideal instability, the increased crash time may be explained by the change in the Alfven time. On the other hand, the magnetic Reynolds number (S) for pellet discharges is about 1/10 ~1/20 of that for gas fuelled discharges. If the sawtooth is due to the m=1 resistive instability and the q-profile for pellet fuelled discharges is similar to that for the gas-fuelled discharges (see Fig.22(b), the growth rate have to increase because of the reduction of S. Experimentally, the sawtooth crash time increases. The observation may mean the sawtooth appeared after the injection is not the resistive mode. For pellet fuelled discharges, the sawtooth crash time tens to increase with increase in line averaged electron density. This tendency may be explained with change in the Alfven time if the sawtooth is triggered by the ideal kink mode.

The reason of the enhanced sawtooth period has not been identified. If the sawtooth period can be described mainly with the resistive diffusion time in the central region, the period for the pellet discharges must be shorter than that for the gas-fuelled discharges, because, generally, the central electron temperature for the pellet discharges are lower than that of the gas-fuelled discharges. The increased sawtooth frequency in Fig.18(a) after the pellet injection can be explained with this scenario. On the other hand, for peaked density (or pressure) profiles the sawtooth period cannot be explained only with the resistive diffusion of the plasma current.

Conclusive results, however, for the reasons of the enhanced sawtooth period and the mechanisms of the sawtooth crash (ideal or resistive) cannot be presented because we do not have the measured data of local shear around the rational surface. The experimental observations are : With increasing $\beta_p{}^l$ or the density gradient in the core region, the sawtooth period increases, the release of the central kinetic energy due to the sawtooth decreases and the sawtooth changes its characteristics from resistive (or reconnecting) type to ideal (non-reconnecting) type.

5. ROTATION OF THE PLASMA CORE

Direction of the m=1 mode rotation on the poloidal cross section is shown in Fig.24. In this discharge, the mode rotation changes the direction during the sawtooth ramping phases (t~7.22, 7.33sec) and at crashes (t~7.265, 7.355sec). From t=7.2 to 7.3s in Fig.24, the m=1 frequency is increased after the sawtooth crash. On the other hand, in Fig. 27, which shows a time history of m=1 mode before and after the sawtooth for a pellet injected Ip=2.8MA discharge (E8985), the m=1 frequency is decreased due tho the sawtooth crash. To understand the change in m=1 frequency during the ramping phase of sawteeth and after the sawtooth crashes, we examined the following analyses.

The frequency and the direction of the m=1 mode change with the balance of co- and counter-injected NBI powers (P_{co} and P_{cntr}) [45]. Figure 28 gives the relationship between the mode

frequency F and M(=(P_{co}-P_{cntr}) / n_e) for gas fuelled phase. The positive sign of F corresponds to the counter direction to the plasma current (toroidally) or the electron diamagnetic direction (poloidally). The linear dependence shown in Fig.28 suggests the mode rotates toroidally and F changes with the toroidal momentum input for gas fuelled discharges. The mode rotation cannot be separated into the toroidal and the poloidal rotations, this is because we have PIN-diode arrays located at only one toroidal section. Figure 29 shows time evolutions of F for two discharges A and B shown in Fig. 28. Before the pellet injection (t<0), mode frequencies for A and B have opposite sign due to the balance of P_{co} and P_{cntr}. After the pellet injection, mode frequencies for A and B change quickly into negative values (Co- or ion-diamagnetic direction) and, then, recovers gradually to their initial values. First changes in F observed 0.7~1.4 sec after the pellet injection correspond to sawtooth-crashes. The mode frequency crosses F=0 during ramping and crashing phases of sawteeth. Change in the direction of rotation during the sawtooth ramp (t~7.22, 7.33sec) in Fig.24 can be understood as a continuous change in F. Due to the sawtooth-crashes, F changes quickly in the direction of Co- or ion-diamagnetic direction. Therefore, if F before the crash is negative, the observed m=1 frequency (|F|) seems to be increased after the crash. Oppositely, if the initial F is sufficiently positive, |F| seems to be decreased by the crash.

If the mode structure is frozen to the fluid motion, the radial electric field E_r due to the v×B field can be calculated with F. Furthermore, if the mode is the resonant one (q=m/n) and the resonant radius (r_s) is identified, E_r can be estimated without separation of F_p (poloidal component of F) and F_t (toroidal component of F). The observed F is written by $F=F_p+F_t$ ($F_p>0$ for electron diamagnetic direction and $F_t>0$ for counter direction.)
If the equilibrium is around axisymmetric configuration, E_r is estimated by (see Fig.30)

$$E_r=\frac{\nabla p_i}{Zne} - v_pB_t+v_tB_p = \frac{\nabla p_i}{Zne} + (F_p 2\pi r_s/m)B_t + (F_t 2\pi R/n)B_p$$

$$= \frac{\nabla p_i}{Zne} + F(2\pi r_s/m)B_t$$

Time evolution of E_r for B (E10814) estimated with using he electron pressure, density measured by Thomson scattering, F and r_s identified with the PIN-diode signals is indicated in Fig.29. After the pellet injection, E_r decreases gradually and reaches about -12kV/m at t=7.0 sec when the stored energy becomes maximum. The discharge E10814 has another coherent mode at r~30~40cm which has an odd poloidal mode number (may be 3) . The frequency of the mode (F*) is also plotted in Fig.29. From t=6.65 to 7.1 sec, the m=1 mode changes its frequency,

whereas F* keeps almost constant values even at the sawtooth-crashes. Therefore, the central core inside the q=1 surface behaves independently of the outer region. This may be an clue to the enhanced confinement inside the q=1 surface.

6. OTHER MHD ACTIVITIES

6.1 "Double Inversion" Sawtoothing Mode

Many of the pellet injected discharges, "double inversion" sawtooth activity is observed in the early phase after the pellet injection. Figure 31 gives an example the double sawtooth (E10814). The sawtooth occurs at t~6.51s. After the sawtooth, the SX-intensity for the medium region (chs.21~18 and chs.27~29; 7<r<21cm) releases the energy and that for the central chords (chs.23~25; r<7cm) and the outer region (r>21cm) receive the energy. This observation suggests that the q-profile is very flat or double-valued [46,47] in the core region of the plasma in the early phase after the pellet injection.

Such "double" sawteeth are sometimes observed for ion cyclotron (IC) heated pellet discharges. For the IC and IC +NB heated discharges, the improvement was observed only when the ion cyclotron resonant surface was located at the plasma center (corresponding to $B_t(0)$=4.3T). For off-axial heating (r~24cm, r_s~20cm) with low power IC of only below ~1MW, increase in W^{DIA} after the pellet injection was drastically suppressed even under the best NB+pellet condition and a double tearing-type sawtoothing mode is observed during the ICRF off-axis (r~24cm) heating near the q=1 rational surface. Figure 32 shows that the double tearing instability is observed during the ICRF heating; the ICRF power was observed to be deposited around ch.9 and ch.10 (r~14 ~21cm) from which the energy was released and the inward and outward heat pulse increases the SX signal at r<14cm (ch.11,12) and r>28cm (ch.8). After Switch-off of the of-axis ICRF heating, the SX signals happen to increase and show the usual sawteeth oscillations. This behavior suggests that the safety factor profile in the central region may be double valued during the ICRF heating.

6.2 Slow Release of The Central Energy

For some pellet-fuelled discharges, the centrally peaked pressure is degraded in a slow time scale compared to that for the sawtooth crash. Figure 33 presents time evolutions of SX-profiles for the energy-decreasing phase for E10814 from t=7.05 to 7.11s (see Figs.17 and 24). The core seems to be displaced to the left hand side of the figure (t=7.05~7.07s), then the central SX-source is released to the outside the q=1 surface (r~35cm). The time scale is several tens of msec, which is much slower than the sawtooth crash time. This time scale is the same order of the resistive time.

whereas F* keeps almost constant values even at the sawtooth-crashes. Therefore, the central core inside the q=1 surface behaves independently of the outer region. This may be an clue to the enhanced confinement inside the q=1 surface.

6. OTHER MHD ACTIVITIES

6.1 "Double Inversion" Sawtoothing Mode

Many of the pellet injected discharges, "double inversion" sawtooth activity is observed in the early phase after the pellet injection. Figure 31 gives an example the double sawtooth (E10814). The sawtooth occurs at t~6.51s. After the sawtooth, the SX-intensity for the medium region (chs.21~18 and chs.27~29; 7<r<21cm) releases the energy and that for the central chords (chs.23~25; r<7cm) and the outer region (r>21cm) receive the energy. This observation suggests that the q-profile is very flat or double-valued [46,47] in the core region of the plasma in the early phase after the pellet injection.

Such "double" sawteeth are sometimes observed for ion cyclotron (IC) heated pellet discharges. For the IC and IC +NB heated discharges, the improvement was observed only when the ion cyclotron resonant surface was located at the plasma center (corresponding to $B_t(0)$=4.3T). For off-axial heating (r~24cm, r_s~20cm) with low power IC of only below ~1MW, increase in W^{DIA} after the pellet injection was drastically suppressed even under the best NB+pellet condition and a double tearing-type sawtoothing mode is observed during the ICRF off-axis (r~24cm) heating near the q=1 rational surface. Figure 32 shows that the double tearing instability is observed during the ICRF heating; the ICRF power was observed to be deposited around ch.9 and ch.10 (r~14 ~21cm) from which the energy was released and the inward and outward heat pulse increases the SX signal at r<14cm (ch.11,12) and r>28cm (ch.8). After Switch-off of the of-axis ICRF heating, the SX signals happen to increase and show the usual sawteeth oscillations. This behavior suggests that the safety factor profile in the central region may be double valued during the ICRF heating.

6.2 Slow Release of The Central Energy

For some pellet-fuelled discharges, the centrally peaked pressure is degraded in a slow time scale compared to that for the sawtooth crash. Figure 33 presents time evolutions of SX-profiles for the energy-decreasing phase for E10814 from t=7.05 to 7.11s (see Figs.17 and 24). The core seems to be displaced to the left hand side of the figure (t=7.05~7.07s), then the central SX-source is released to the outside the q=1 surface (r~35cm). The time scale is several tens of msec, which is much slower than the sawtooth crash time. This time scale is the same order of the resistive time.

Figure 34 is another example for the slow release of the central energy. The figure shows the time evolution of the SX-intensity for two chords of r=0 and r~2/3a for a 2.1MA limiter discharge E8120 (the SX-profiles were shown in Fig.5). Pellets were injected at t~6.0s, then the SX-intensity increased strongly in the central region. At t~6.53s, the central core happened to be displaced and a large m=1 oscillation started, then the central sx-intensity decreased slowly. During the decay phase, the spatial distribution of the m=1 character did not change (see Fig.35), therefore the slow release is not due to the slow change of the current profile.

The release may be due to the ballooning instability or the enhanced transport because of the m=1 displacement. However, the clear interpretation of the slow release of the central energy has not been acquired yet.

6.3 Large m=2 Oscillation

Figure 36 shows an example of the m=2 oscillation enhanced by the pellet injection. In this case, pellets were injected just after the ramp-up phase of the plasma current, therefore, the current profile is relatively flatter than usual target plasma of the pellet injection. A large coherent mode starts just after the second pellet injected at t=2.48sec (Fig. 36(a)). Figure 36(b) gives the structure of the mode. Based on the mode pattern, the poloidal mode number of the fluctuation can be identified as a m=2 mode. The spatial distribution of the soft-X ray intensity is shown in Fig.36 (c), where a large amount of the soft-X ray source is observed around ch.9~16 (r=53~28cm). Figure 36(d) shows time traces of the line integrated electron density measured with two FIR interferometers viewing vertically at r=50 cm and r=-50cm. Both density fluctuations are in-phase, which supports the poloidal mode number is even. With these results, a large amount of the injected density is trapped inside the m=2 island and the particle confinement is much better (~1~2 orders of magnitude) inside the island than outside the island.

7. SUMMARY

Improved energy confinement for the pellet fuelled plasmas on JT-60 is mainly due to the peaked density and pressure profiles inside the q=1 rational surface, where the confinement characteristics appear to be better than those in the outer (q>1) region. In the well-center-fuelled pellet injection discharges, the sawtooth activity can be suppressed completely during 0.4~1 sec or the frequency of sawteeth are reduced by up to one order of magnitude during 0.5~1.5 sec after the pellet injection. For high-current low-q (I_p=2.5~3.1MA; q(a)<3) discharges, reduction in the sawtooth frequency has a strong relationship with enhanced confinement and peakedness of the electron density profile. The contribution of the sawtooth activity to the global energy confinement increases systematically with decreasing q(a).

Figure 34 is another example for the slow release of the central energy. The figure shows the time evolution of the SX-intensity for two chords of r=0 and r~2/3a for a 2.1MA limiter discharge E8120 (the SX-profiles were shown in Fig.5). Pellets were injected at t~6.0s, then the SX-intensity increased strongly in the central region. At t~6.53s, the central core happened to be displaced and a large m=1 oscillation started, then the central sx-intensity decreased slowly. During the decay phase, the spatial distribution of the m=1 character did not change (see Fig.35), therefore the slow release is not due to the slow change of the current profile.

The release may be due to the ballooning instability or the enhanced transport because of the m=1 displacement. However, the clear interpretation of the slow release of the central energy has not been acquired yet.

6.3 Large m=2 Oscillation

Figure 36 shows an example of the m=2 oscillation enhanced by the pellet injection. In this case, pellets were injected just after the ramp-up phase of the plasma current, therefore, the current profile is relatively flatter than usual target plasma of the pellet injection. A large coherent mode starts just after the second pellet injected at t=2.48sec (Fig. 36(a)). Figure 36(b) gives the structure of the mode. Based on the mode pattern, the poloidal mode number of the fluctuation can be identified as a m=2 mode. The spatial distribution of the soft-X ray intensity is shown in Fig.36 (c), where a large amount of the soft-X ray source is observed around ch.9~16 (r=53~28cm). Figure 36(d) shows time traces of the line integrated electron density measured with two FIR interferometers viewing vertically at r=50 cm and r=-50cm. Both density fluctuations are in-phase, which supports the poloidal mode number is even. With these results, a large amount of the injected density is trapped inside the m=2 island and the particle confinement is much better (~1~2 orders of magnitude) inside the island than outside the island.

7. SUMMARY

Improved energy confinement for the pellet fuelled plasmas on JT-60 is mainly due to the peaked density and pressure profiles inside the q=1 rational surface, where the confinement characteristics appear to be better than those in the outer (q>1) region. In the well-center-fuelled pellet injection discharges, the sawtooth activity can be suppressed completely during 0.4~1 sec or the frequency of sawteeth are reduced by up to one order of magnitude during 0.5~1.5 sec after the pellet injection. For high-current low-q (I_p=2.5~3.1MA; q(a)<3) discharges, reduction in the sawtooth frequency has a strong relationship with enhanced confinement and peakedness of the electron density profile. The contribution of the sawtooth activity to the global energy confinement increases systematically with decreasing q(a).

For higher-q and lower-$\beta_p{}^1$ discharges in JT-60, the sawtooth crash behaves following the fully reconnecting style. Such sawteeth often have precursor m=1 oscillation and very small or no successor oscillation. In contrast, for lower-q and higher-$\beta_p{}^1$ discharges, the sawtooth crash tends to follow incomplete reconnection and the successor oscillation becomes larger: With increasing $\beta_p{}^1$ or the density gradient in the core region, the sawtooth period increases, the release of the central kinetic energy due to the sawtooth decreases and the sawtooth changes its characteristics from resistive (or reconnecting) type to ideal (non-reconnecting) type.

The rotation velocity of the central plasma column after the pellet injection is also discussed with the frequencies of the m=1 oscillations. Just after the pellet injection, the plasma column starts to rotate in the ion-diamagnetic direction or the co-direction to the plasma current. At each sawtooth, the rotation frequency changes suddenly to the ion-diamagnetic direction or the co-direction.

ACKNOWLEDGEMENT

The authors would like to gratefully thank Drs. M. Yoshikawa, T.Iijima, S. Tamura and Y.Shimomura for their continuous encouragement.

For higher-q and lower-$\beta_p{}^1$ discharges in JT-60, the sawtooth crash behaves following the fully reconnecting style. Such sawteeth often have precursor m=1 oscillation and very small or no successor oscillation. In contrast, for lower-q and higher-$\beta_p{}^1$ discharges, the sawtooth crash tends to follow incomplete reconnection and the successor oscillation becomes larger: With increasing $\beta_p{}^1$ or the density gradient in the core region, the sawtooth period increases, the release of the central kinetic energy due to the sawtooth decreases and the sawtooth changes its characteristics from resistive (or reconnecting) type to ideal (non-reconnecting) type.

The rotation velocity of the central plasma column after the pellet injection is also discussed with the frequencies of the m=1 oscillations. Just after the pellet injection, the plasma column starts to rotate in the ion-diamagnetic direction or the co-direction to the plasma current. At each sawtooth, the rotation frequency changes suddenly to the ion-diamagnetic direction or the co-direction.

ACKNOWLEDGEMENT

The authors would like to gratefully thank Drs. M. Yoshikawa, T.Iijima, S. Tamura and Y.Shimomura for their continuous encouragement.

REFERENCES

[1] KAMADA,Y., YOSHINO,R.,NAGAMI,M.,OZEKI,T., HIRAYAMA,T., et al. Nucl. Fusion **29** (1989) 1785.

[2] JT-60 Team presented by NAGAMI,M., Plasma Phys. Control. Fusion **31,** (1989) 1597

[3] USHIGUSA, K., et al., 'Lower Hybrid Wave Heating in Peaked Density Plasmas Produced by Pellet Injections on JT-60', to be submitted to Nucl. Fusion

[4] JT-60 Team ' Review of JT-60 Experimental Results from June to October, 1988' JAERI-M 89-033.

[5] YOSHINO, R., et al. to be submitted to Nucl. Fusion

[6] MILORA,S.L., FOSTER,C.A., THOMAS,C.E., BUSH,C.E., WILGEN,J.B., *et al.*, Nucl. Fusion **20** (1980) 1491.

[7] GREENWALD,M., GWINN,D., MILORA,S., PARKER,J., PARKER,R., *et al.*, in *Plasma Physics and Controlled Nuclear Fusion Research* (Proc.10th Int. Conf., London, 1984) Vol.I, (IAEA, Vienna, 1985) ,45. or Phys. Rev. Lett. **53** (1984) 352.

[8] SENGOKU,S., ABE,M., HOSHINO,K., ITOH, K., KAMEARI,A., *et al.*, in *Plasma \ Physics and Controlled Nuclear Fusion Research* (Proc. 10th Int. Conf., London, 1984) Vol.I, (IAEA, Vienna, 1985) ,405.

[9] TFR GROUP, Nucl. Fusion **27** (1987) 1975.

[10] KAUFMANN,M., BEHRINGER,K., FUSSMANN,G., GRUBER,O., LACKNER,K., *et al.*, in *Plasma Physics and Controlled Nuclear Fusion Research* (Proc.12th Int. Conf., Nice, 1988) IAEA-CN-50/ A-4-2.

[11] KASAI,S., MIURA,Y., HASEGAWA,K. and SENGOKU,S. "Review: Study of Single Pellet Injection Experiments and Development of Pellet Injector in JFT-2M" JAERI-M 87-161 Japan Atomic Energy Research Institute (1987).

[12] SHMIDT,G.L., MILORA.S.L., ARUNASALAM,V., BELL,M.G., BITTER,M., *et al.*, in *Plasma Physics and Controlled Nuclear Fusion Research* (Proc.11th Int. Conf., Kyoto, 1986) Vol.I, (IAEA, Vienna, 1987) ,171.

[13] The JET Team presented by SCHMIDT,G.L., in *Plasma Physics and Controlled Nuclear Fusion Research* (Proc. 12th Int. Conf., Nice, 1988) IAEA-CN-50 / A-IV-1.

[14] VON GOELER, S., STODIEK,W., SAUTHOFF,N., Phys. Rev. Lett. **33** (1974) 1201.

[15] WESSON, J., ' Theory of Sawtooth Oscillations', JET-P(87)55, 1987.

[16] WESTERHOF.E., Comments Plasma Phys. Controlled Fusion **11** (1987) 79.

[17] McGUIRE, K., ARUNASALAM, V., BELL, M.G., et al. in *Plasma Physics and Controlled Nuclear Fusion Research* (Proc.11th Int. Conf., Kyoto, 1986) Vol.I, (IAEA, Vienna, 1987) ,421.

[18] CAMPBELL, D. J., GILL, R.D., GOWERS,C.W., et al. Nucl Fusion **26** (1986) 1085.

[19] ISHIDA,S., SHIRAI,H., NAGASHIMA,K., et al. Plasma Phys. Controll. Fusion **30** (1988) 1069.

[20] TSUJI, S., et al., Nucl Fusion **25** (1985) 205.

[21] NAGAYAMA,Y., TSUJI,S., KAWAHATA,K., Phys. Rev. Lett. **61** (1989) 1839.

[22] JANICKI,C., DECOSTE,R., SIMM,C., Phys. Rev. Lett. **62** (1989) 3038.

[23] YAMAMOTO,S., MAENO, M., SUZUKI,N., AZUMI,M., et al., Nucl Fusion **21** (1981) 993.

[24] ISHIDA,S., NAGASHIMA,K., NISHITANI,T., et al. Nucl. Fusion **30** (1990) 552.

[25] Many papers have been reported from JET. For example see CAMPBELL,D.J., CORDEY,J.G., EDWARDS,A.W., et al., in *Plasma Physics and Controlled Nuclear Fusion Research* (Proc. 12th Int. Conf., Nice, 1988) IAEA-CN-50/ A-VII-2.

[26] McCORMICK,K., SOLDNER,F.X., ECKHARTT,D., et al., Phys. Rev. Lett. **58** (1987) 491.

[27] HOSEA,J., WILSON,J.R., HOOKE,W., et al., Plasma Phys. Controll. Fusion **28** (1986) 1241.

[28] KNOWLTON,S., PORKOLAB,M. and TAKASE,Y., Nucl Fusion **28** (1988) 99.

[29] NAITO, O., et al., to be submitted to Nucl. Fusion

[30] SILLEN, R.M., PIEKAAR,H.W., OYEVAAR,T., et al., Nucl Fusion **26** (1986) 303.

[31] SNIDER,R.T., CONTENT,D., JAMES,R., et al., Phys. Fluids B **1** (1989) 404.

[32] SNIPES,J.A., and GENTLE,K.W., Nucl Fusion **26** (1986) 993.

[33] CAMPBELL,D.J., EDWARDS,A.W., and PEARSON,D., in in *Control. Nucl. Fusion and Plasma Physics* (Proc. 16th Europ. Conf., Venice, 1989), Vol.I, (1989) 509.

[34] SOLTWISCH,H., STODIEK,W., MANICKAM,J., et al., in *Plasma Physics and Controlled Nuclear Fusion Research* (Proc.11th Int. Conf., Kyoto, 1986) Vol.I, (IAEA, Vienna, 1987), 263.

[35] COPPI,B., HASTIE,R.J., MIGLIUOLO,S., et al., Phys. Lett., A **132** (1988) 267.

[36] WHITE,R.B., BUSSAC,M.N., ROMANELLI,F., Phys. Rev. Lett. **62** (1989) 539.

[37] OZEKI, T., AZUMI,M., KAMADA,Y., YOSHINO,R., et al. submitted to Nucl. Fusion

[38] YOSHINO, R. Nucl. Fusion **29** (1989) 2231.

[39] Naito, O. and JT-60 Team, Nucl. Fusion **30** (1990) 195.

[40] McGUIRE,K.M., BUCHSE,R., CAVALLO,A., et al., in in *Control. Nucl. Fusion and Plasma Physics* (Proc. 16th Europ. Conf., Venice, 1989), Vol.I, (1989) 477.
[41] KADOMTSEV,B.B., Sov. J. Plasma Phys. **1** (1975) 389.

[42] BUSSAC,M.N., PELLAT,R., EDERY,D., and SOULE,J.L., Phys. Rev. Lett. **35** (1975) 1638.

[43] WELLER,A., CHEETHAM,A.D., EDWARDS,A.W., et al., Phys. Rev. Lett. **59** (1987) 2303.

[44] WESSON,J.A. Plasma Phys. Controll. Fusion **28** (1986) 243.

[45] ISHIDA,S., NISHITANI,T., NAGASHIMA,K., et al., Nucl. Fusion **28** (1988) 2225.

[46] PFEIFFER,W., Nucl. Fusion **25** (1985) 673.

[47] YAMADA,H., McGUIRE,K., COLCHIN,D., et al., "Compound Sawtooth Study in Ohmically Heated TFTR Plasmas", Rep. PPPL-2213, Princeton Plasma Physics Lab., Princeton, NJ (1985).

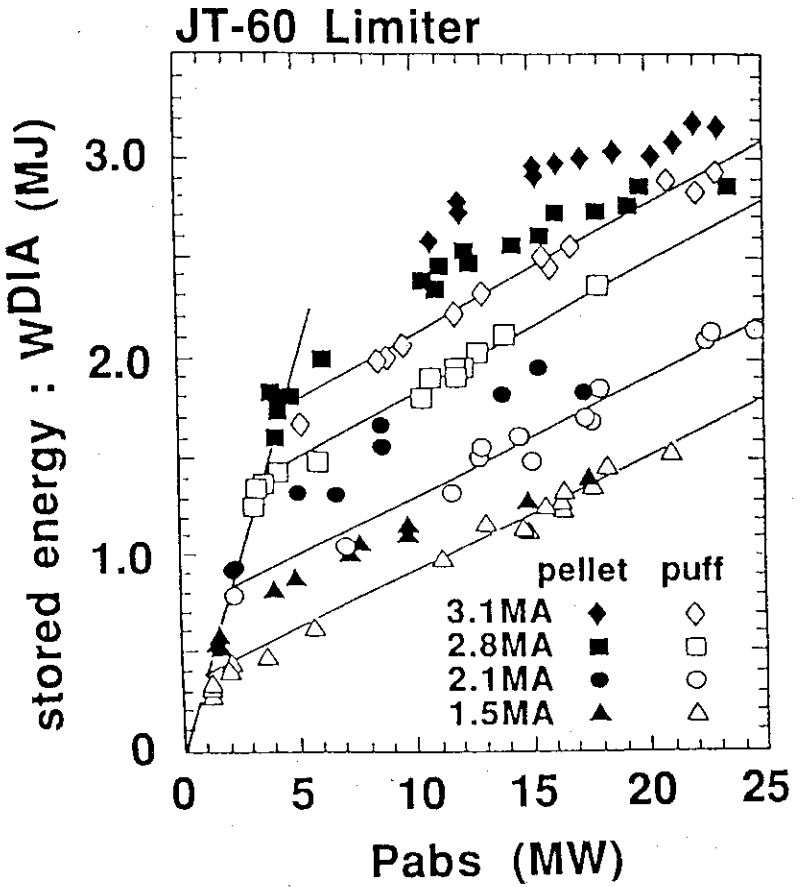

Fig. 1
Relationship between the stored energy measured with a diamagnetic loop W^{DIA} and the absorbed power P_{abs} for NB heated limiter discharges with the plasma current I_p of 1.5, 2.1, 2.8 and 3.1MA. Data for pellet fuelled discharges are shown by closed symbols. For each I_p and P_{abs}, only the pellet cases having the highest improvement are plotted.

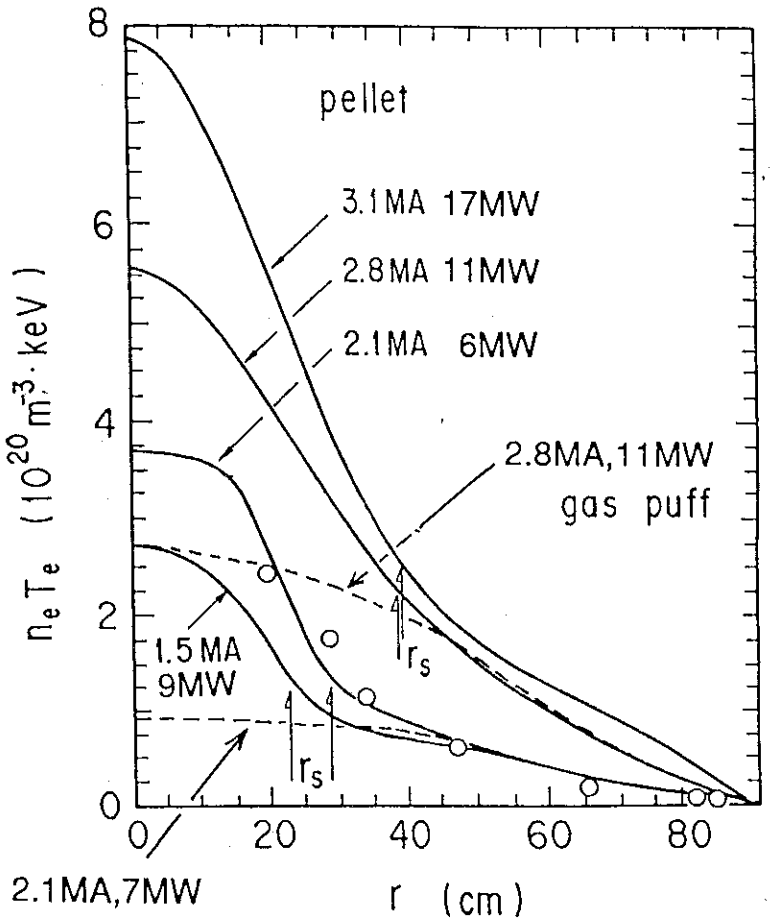

Fig. 2
Electron pressure p_e ($n_e \times T_e$) profiles for pellet fuelled discharges (I_p=3.1, 2.8, 2.1 and 1.5MA, safety factors at the plasma surface q(a)=2.3, 2.3, 3.3 and 4.2), gas fuelled reference data (I_p=2.8 and 2.1MA) and positions of the q=1 rational surfaces (r_s) determined with the sawtooth inversion radii. The electron pressure profiles were constructed with combinations of Thomson scattering, ECE and soft-X ray emission (SX) data.

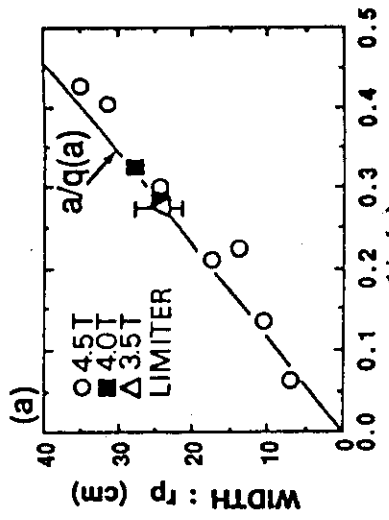

Fig. 4 Results of scan of I_p (0.5~3.1MA) and B_t (3.5~4.8T) to survey the dependence of the width of the peaked portion of the electron pressure (r_p) on q(a). The solid line in (a) indicating r_s for gas fuelled discharges is written by r_s=a/q(a). (b) shows the soft-X ray emission profiles ($\sim p_e^2$) normalized by the central values for three cases with different q(a) and gives the definition of r_p. The width (r_p) increases linearly with 1/q(a) and the values agree systematically with the q=1 surface (r_p=r_s).

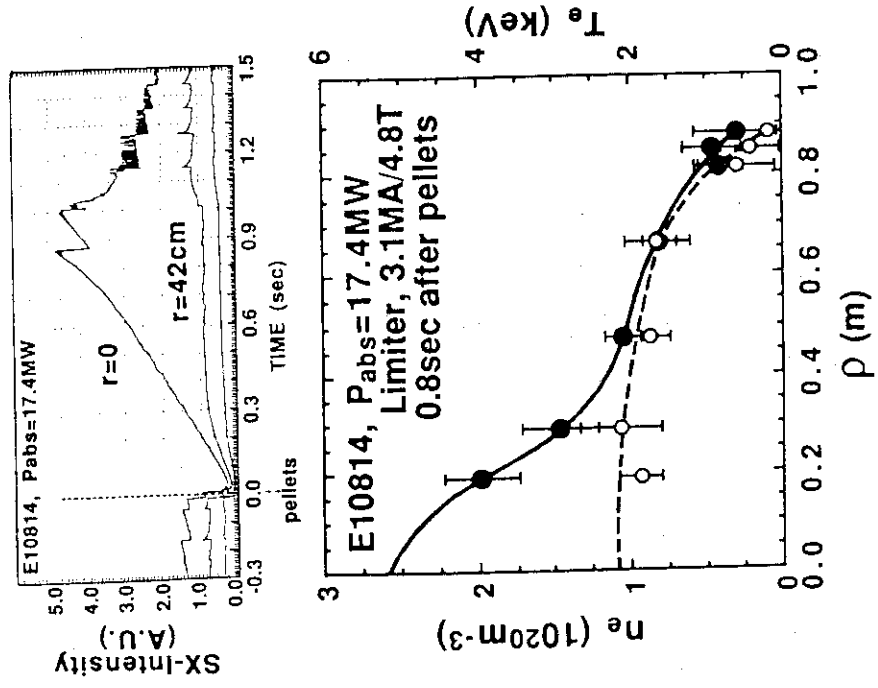

Fig. 3 : $n_e(r)$ and $T_e(r)$ measured at 0.8 sec after the pellet injection for a 3.1MA limiter discharge (Bt=4.8T, q(a)=2.3).The peaking of the electron pressure profile is due to the peaked electron density profile. The figure also shows time evolutions of soft-X ray intensity for two chords of r=0 and 42 cm. In this case, the sawtooth repetition time in the pre-pellet portion is 80~100 msec and the sawtooth activity is suppressed completely during ~0.8sec after the pellet injection.

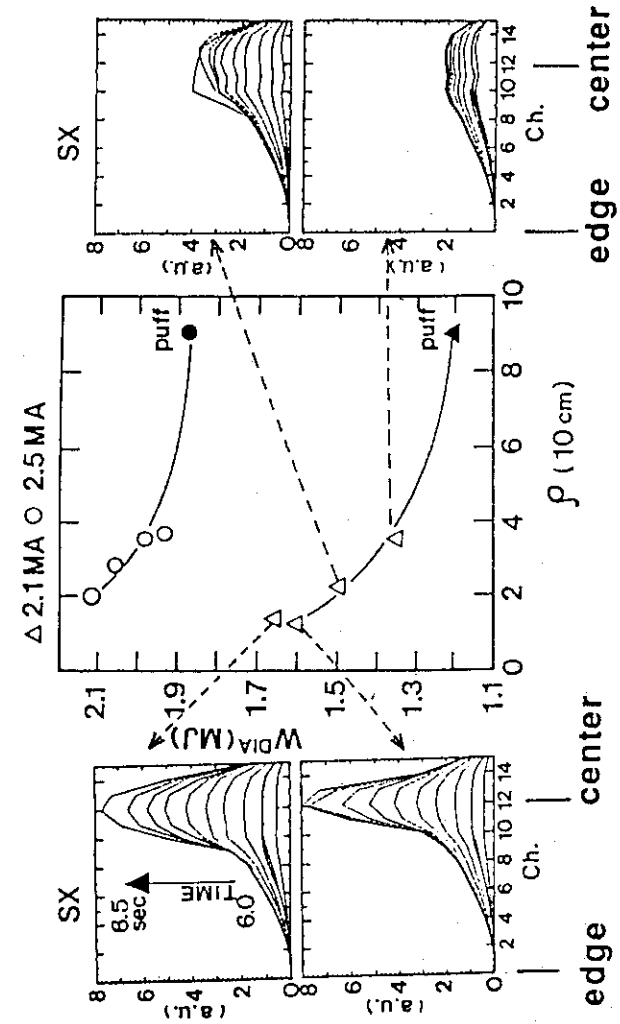

Fig. 6
Dependence of WDIA on the penetration depth from the axis measured with the pellet monitor for 2.1 and 2.5 MA discharges. For both sets, four pellet-injected and a gas-puffed shots with the same P_{abs} of 10MW are included. Time evolutions of the SX profiles for the four 2.1 MA discharges are also given.

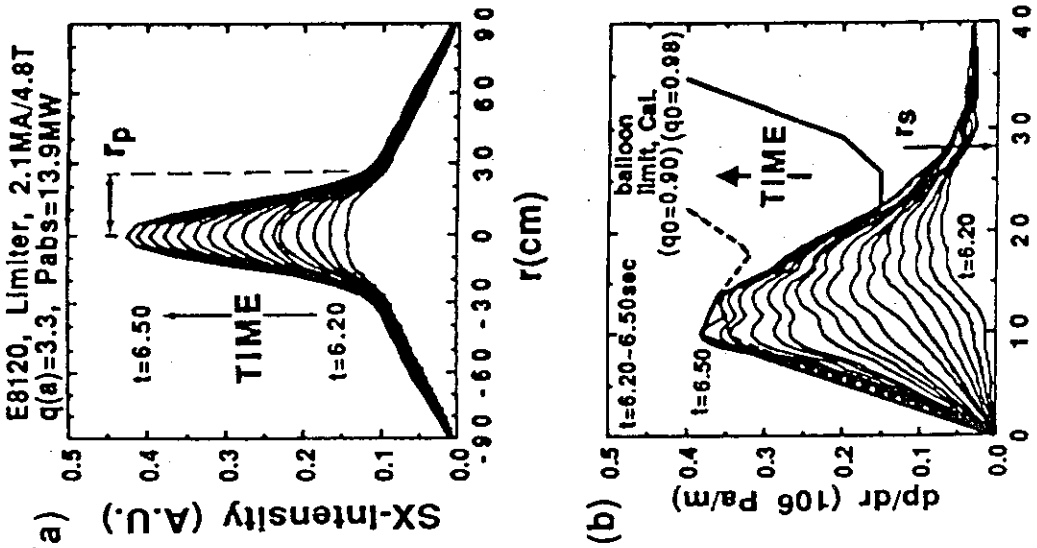

Fig. 5
Time evolution for the profiles of Abel inverted SX emission (a) and those of electron pressure gradient estimated with SX signals (b) for a 2.1MA limiter discharge heated by NB (P_{abs}=13MW). Pellets were injected at t=6.0sec. The SX-profile peaks strongly inside r_s. During the pressure peaking phase, the p(r) profile evolves only inside r_s and the position is kept almost constant (r_s~28cm). At first, the saturation occurs locally at the outer portion inside r_s, then the pressure gradient reaches the limiting value in the inner region. In (b), the calculated balloon-limits are drawn for two cases with assumed q(0) of 0.98 and 0.90.

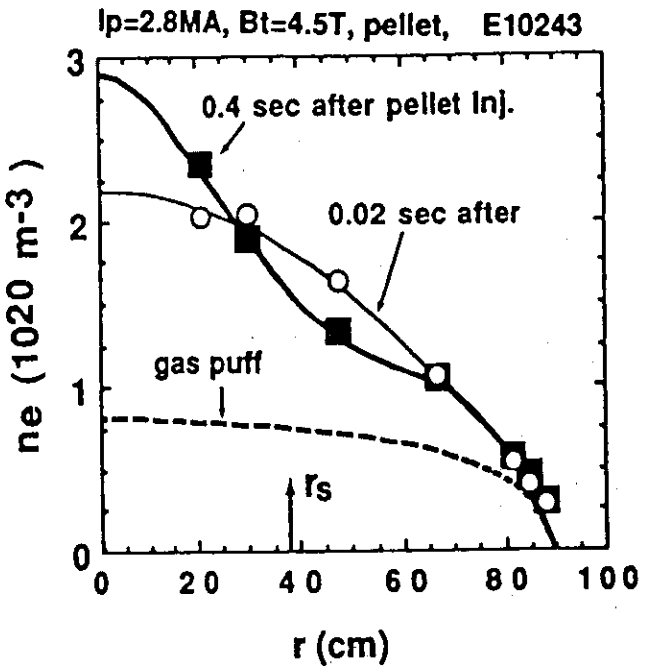

Fig. 7
$n_e(r)$ for 0.02 and 0.4 sec after the pellet injection and that for the gas fuelling (before the injection). At 0.02 sec after the injection, n_e profile is broad. At 0.4 sec after the pellets, the n_e profile peaks inside r_s. The particle confinement inside r_s seems to be better than that in the outer region.

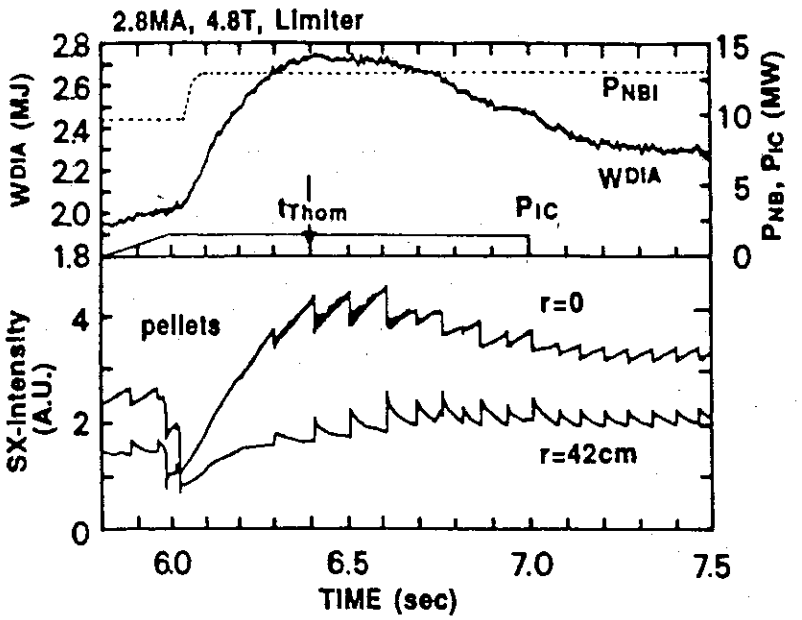

Fig. 8
Time evolutions of W^{DIA} and the SX emission for the central and r=42cm chords for a 2.8MA limiter discharge E10324 (q(a)=2.35). In this case, the sawtooth activity is not suppressed completely after the pellet injection.

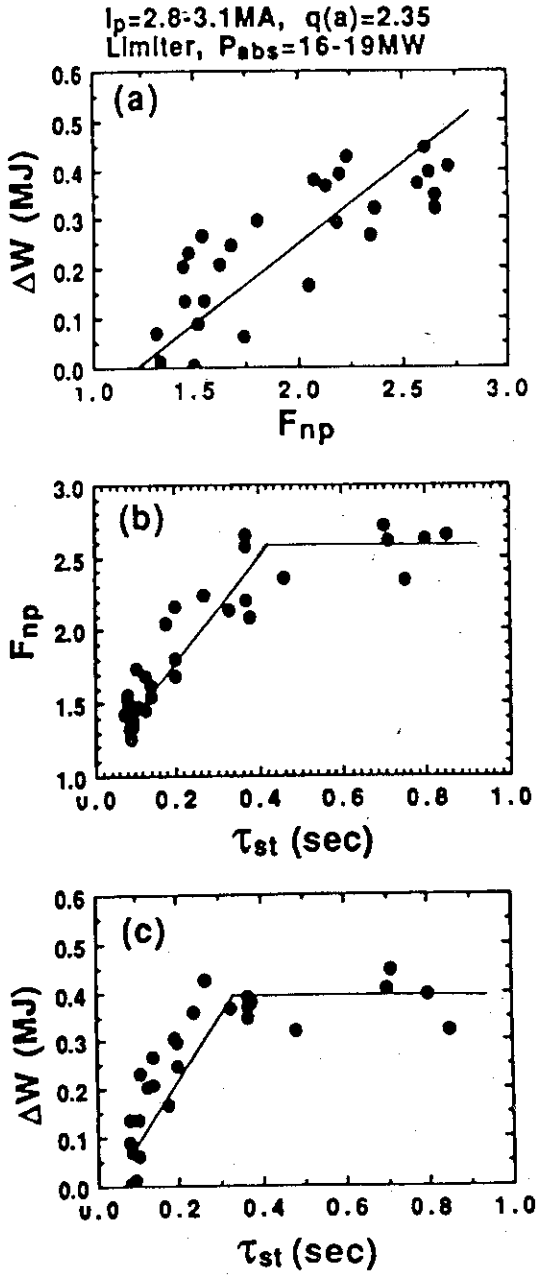

Fig. 9
Relationships among ΔW (improvement in the stored energy compared to the gas fuelled scaling), peaking factors of the n_e profiles (F_{np}) and the averaged sawteeth periods (τ_{st}) for I_p/B_t=2.8MA/4.5T and 3.1MA/4.8T limiter discharges with P_{abs} of 16~19MW and q(a)~2.35.

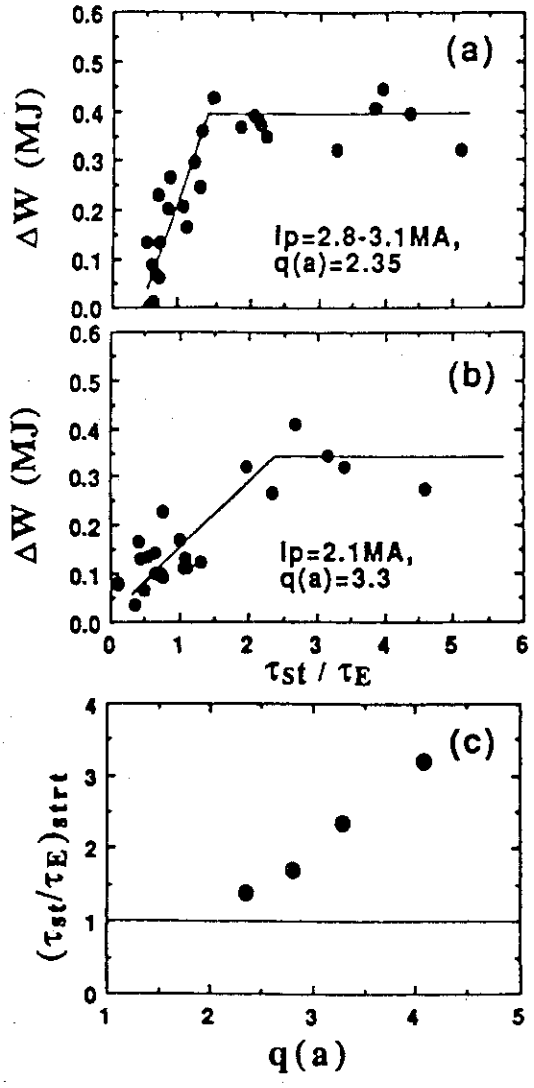

Fig. 10
Dependence of ΔW on the sawtooth period τ_{st} normalized by τ_E. In (a), saturation occurs at τ_{st}~1.4τ_E and further improvement cannot be obtained for τ_{st}>1.4τ_E. (b) corresponds to the data with I_p=2.1MA (q(a)=3.3). In this case, the saturation occurs at τ_{st}/τ_E ~2.5. (c) gives the relationship between q(a) and τ_{st}/τ_E at the saturation point, $(\tau_{st}/\tau_E)_{strt}$, obtained in some data sets with different I_p.

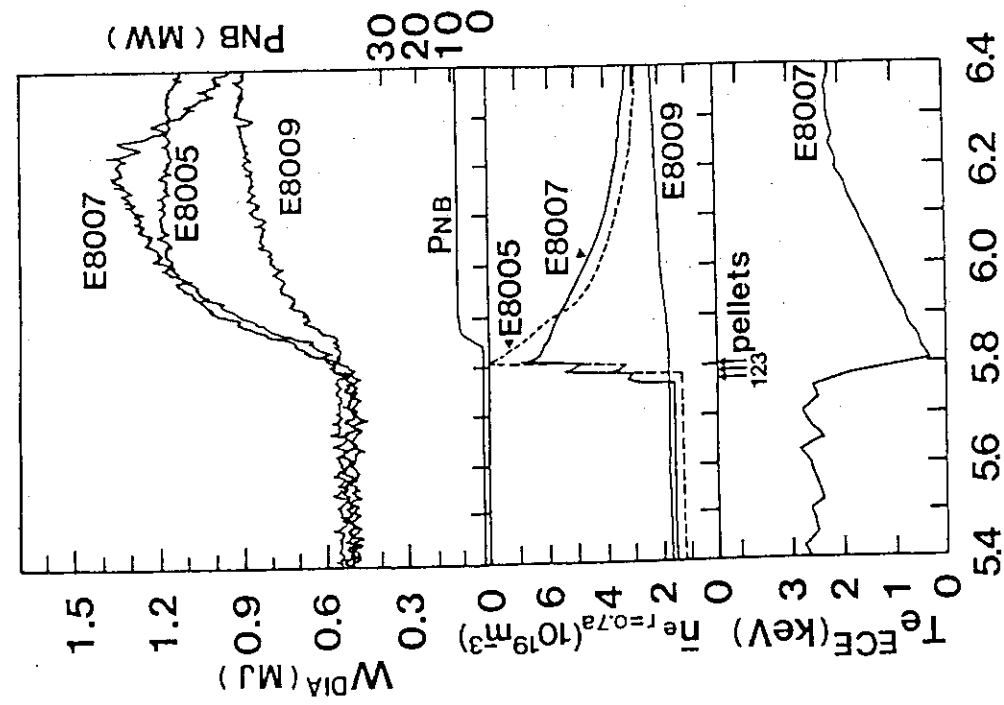

Fig. 11
Comparison of plasma parameters among gas fuelled (E8009), two-pellet (E8005) and tree-pellet injected (E8007) 1.8MA lower X-point discharges at the same Pabs of 9.5MW. The stored energy for E8007 takes the maximum value at t=6.2 sec when $T_e(0)$ almost recovers to its initial value and decays simultaneously with the onset of a large sawtooth (shown later in Fig. 13).

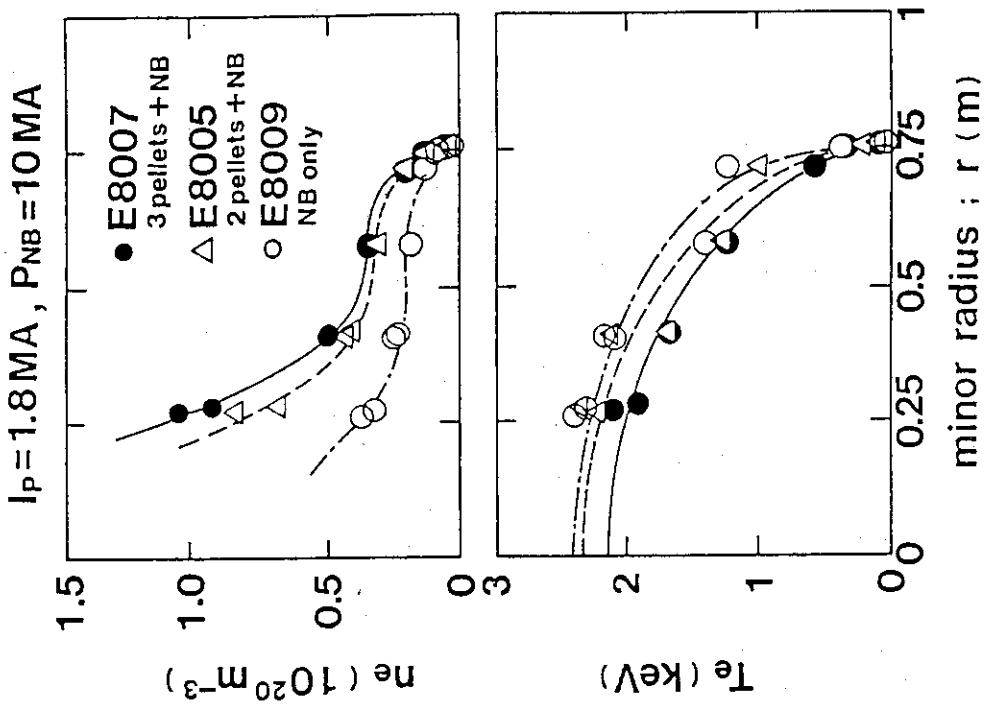

Fig. 12
Profiles of n_e and T_e for the three discharges measured at t=6.2sec (0.4 sec after the pellet injection) with the Thomson scattering system. The Te profiles for E8007 and E8005 have almost the same values with that for E8009, while $n_e(r)$ for the pellet discharges are kept much higher than that for the gas fuelled shot especially in the core region.

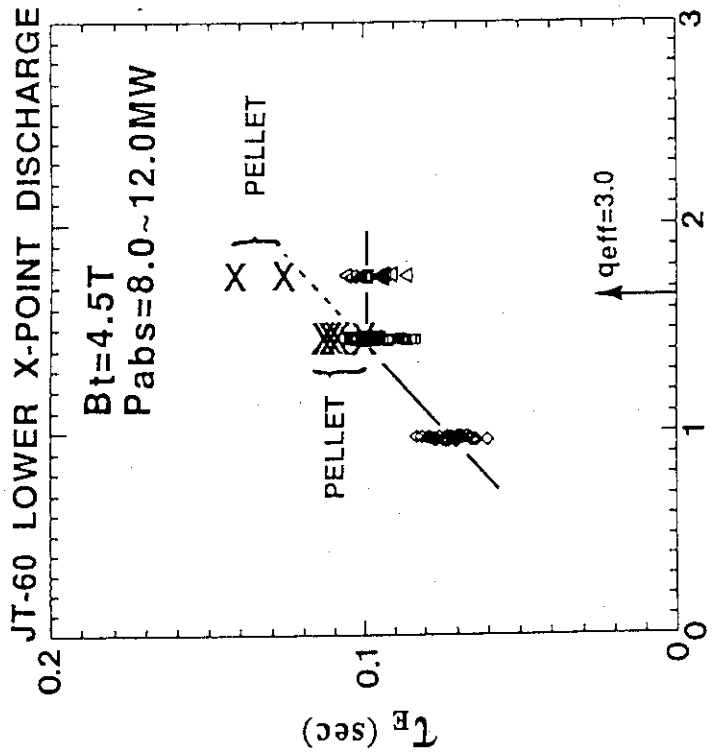

Fig. 14
The energy confinement time τ_E for the pellet and gas fuelled discharges (B_t=4.5T,P_{abs}=8~12MW) are shown as a function of I_p. For the gas fuelled lower-x point discharges, the increase in τ_E with I_p is degraded at qeff<3. While, for the pellet discharges, τ_E increases linearly with I_p at qeff<3 and the improvement by the pellet injection is distinct in the low-q regime (I_p=1.8MA).

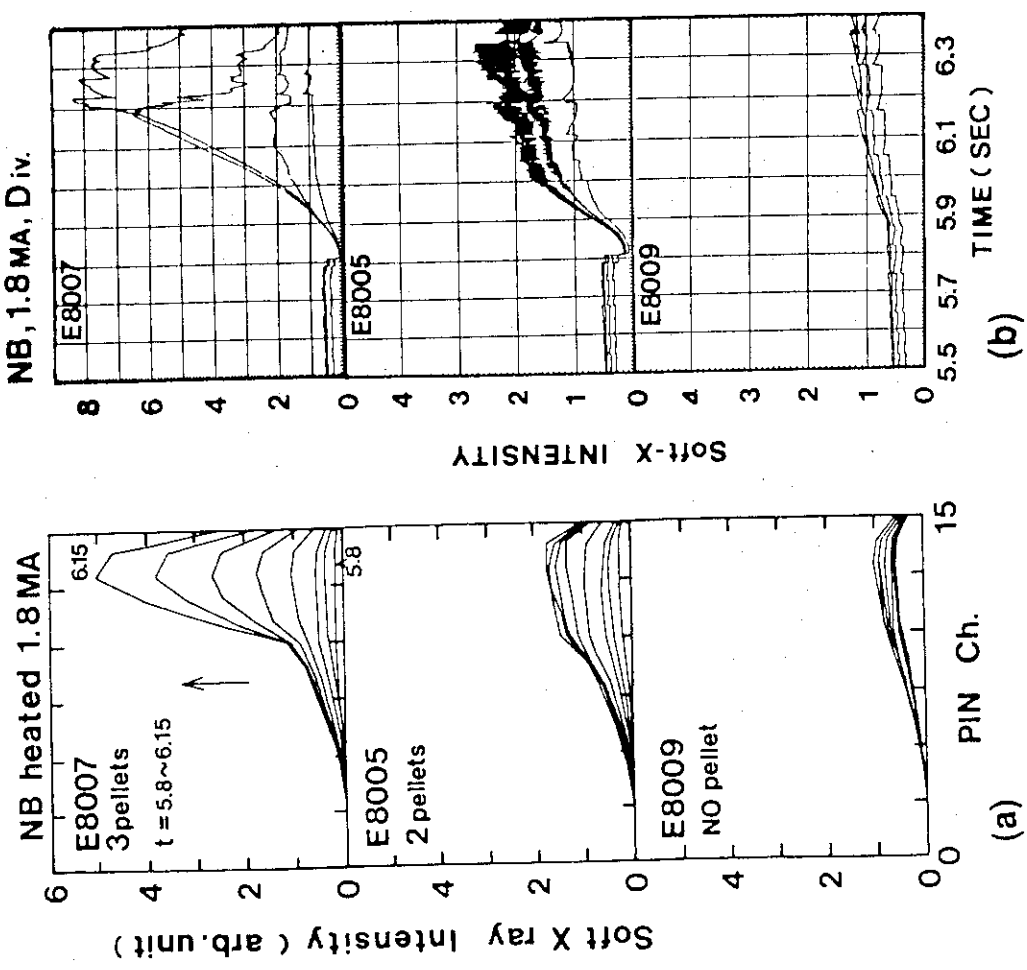

Fig. 13 :
(a) and (b) show time evolutions of spatial distribution and those for the 4 chords near the magnetic axis, respectively. The SX profile for E8007 peaks strongly in a region inside Ch.10 (~r_s). In turn, for E8005, the profile is flat in this region.

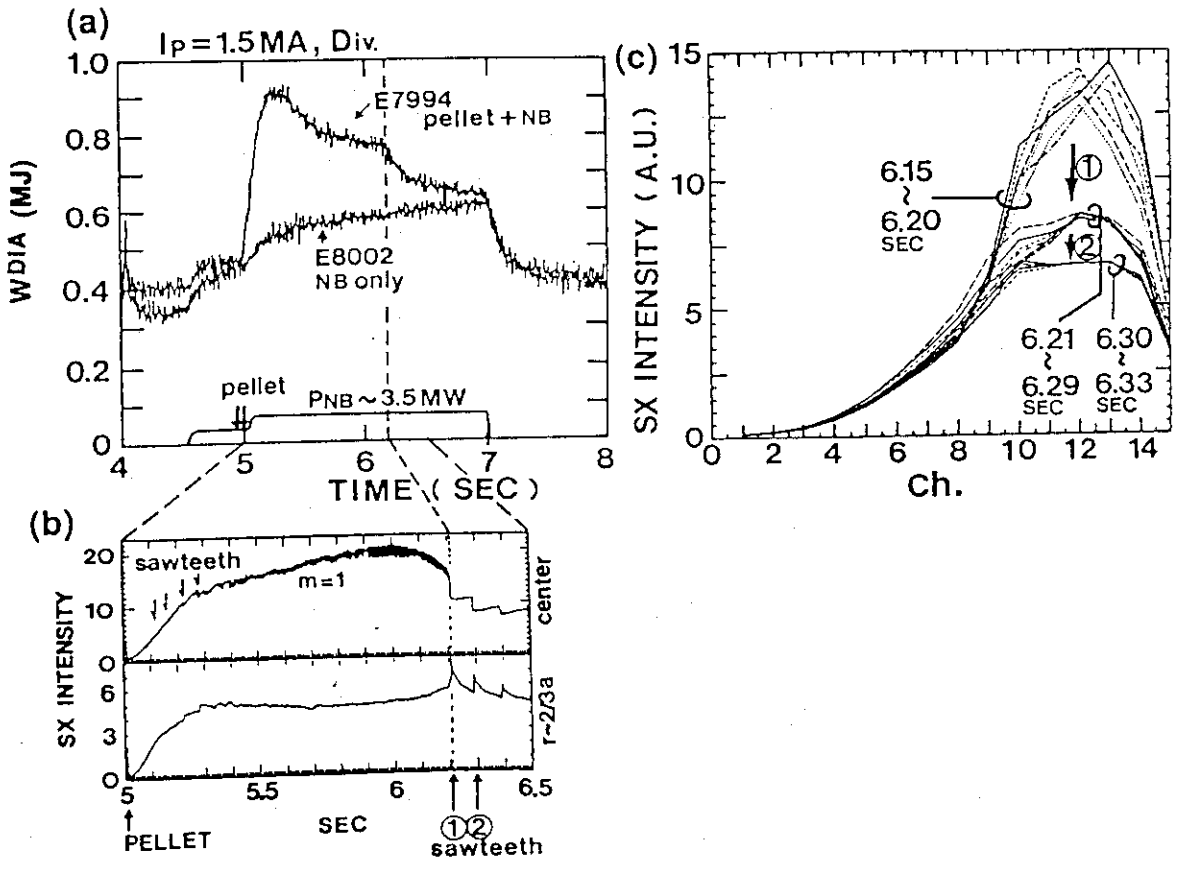

Fig. 15
(a) compares traces of W^{DIA} for a pellet fuelled (E7994) and a gas fuelled (E8002) 1.5MA lower-x point discharges with P_{NB} of 3.5MW. From t=6.2 sec, W^{DIA} for the pellet shot decreases rapidly to the gas fuelled level. The sudden decrease in W^{DIA} occurs simultaneously with the onset of the first large sawtooth after the pellet injection.
(b) shows the time traces of SX emission rate for two chords seeing the center and r~2/3a for E7994. (c)The strongly peaked SX-profile is broadened at each sawtooth crash.

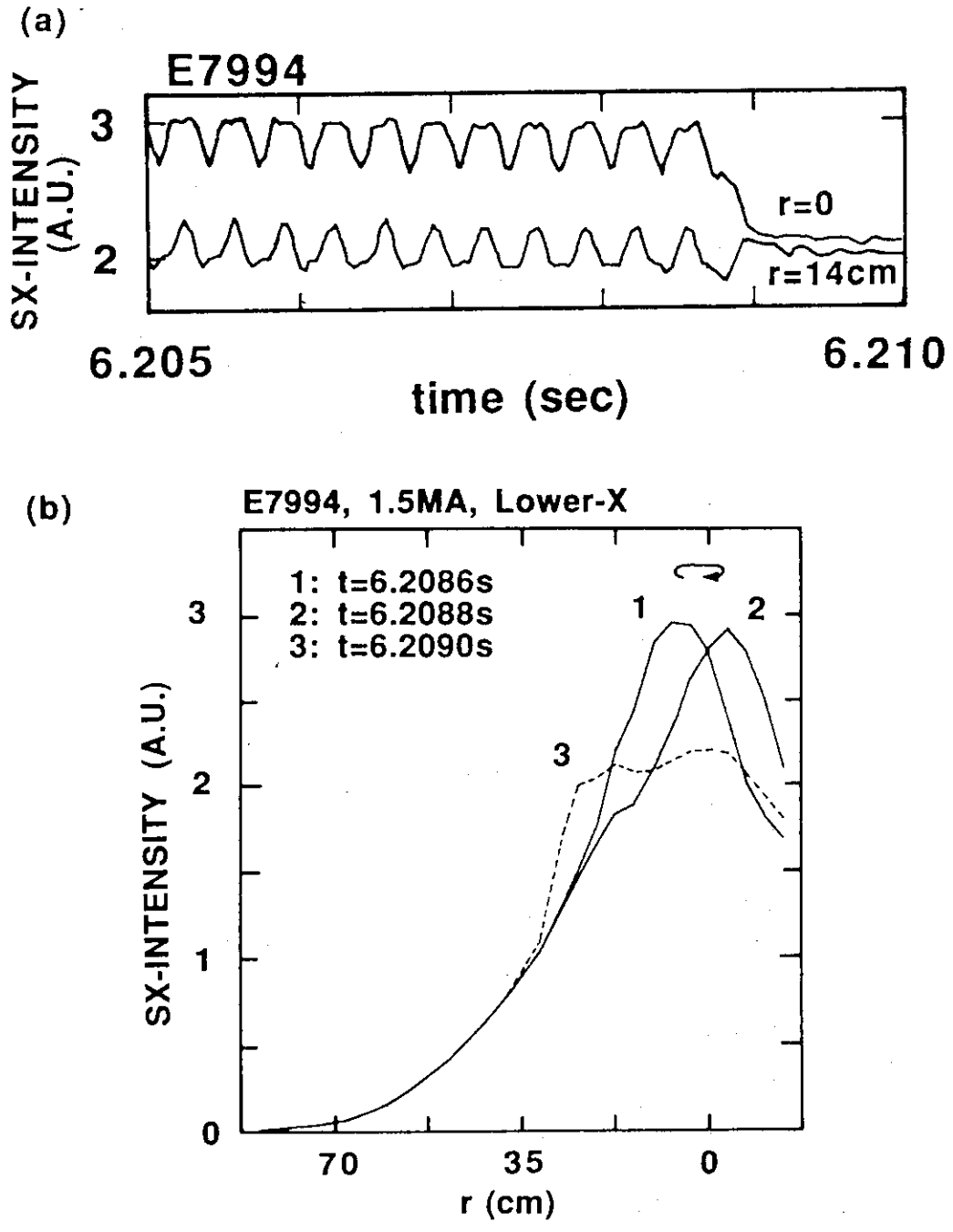

Fig. 16
(a): Evolutions of the SX-signals around the first large sawtooth for E7994. For this crash, only the pre-cursor m=1 oscillation is observed and the m=1 structure disappears after the crash . (b): The centrally peaked portion of the SX-profile is released outward within 150 μsec and the produced profile is almost flat inside the mixing radius.

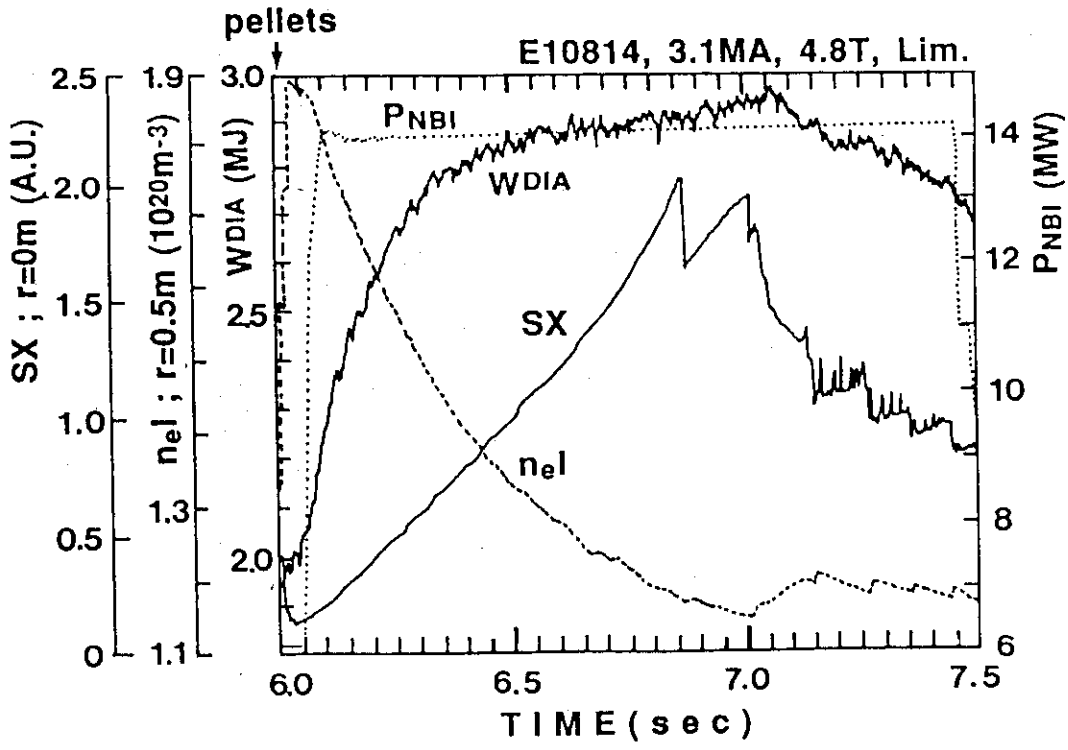

Fig. 17
Time evolutions of W^{DIA}, $n_e l$ (r~0.5m), soft-X ray intensity (central chord) for a pellet fuelled 3.1MA limiter discharge (E10814). Pellets were injected at t~6.0 sec. At the first and the second sawteeth at t=6.82 sec and 7.05 sec, the total stored energy is not affected by the sawteeth crashes.

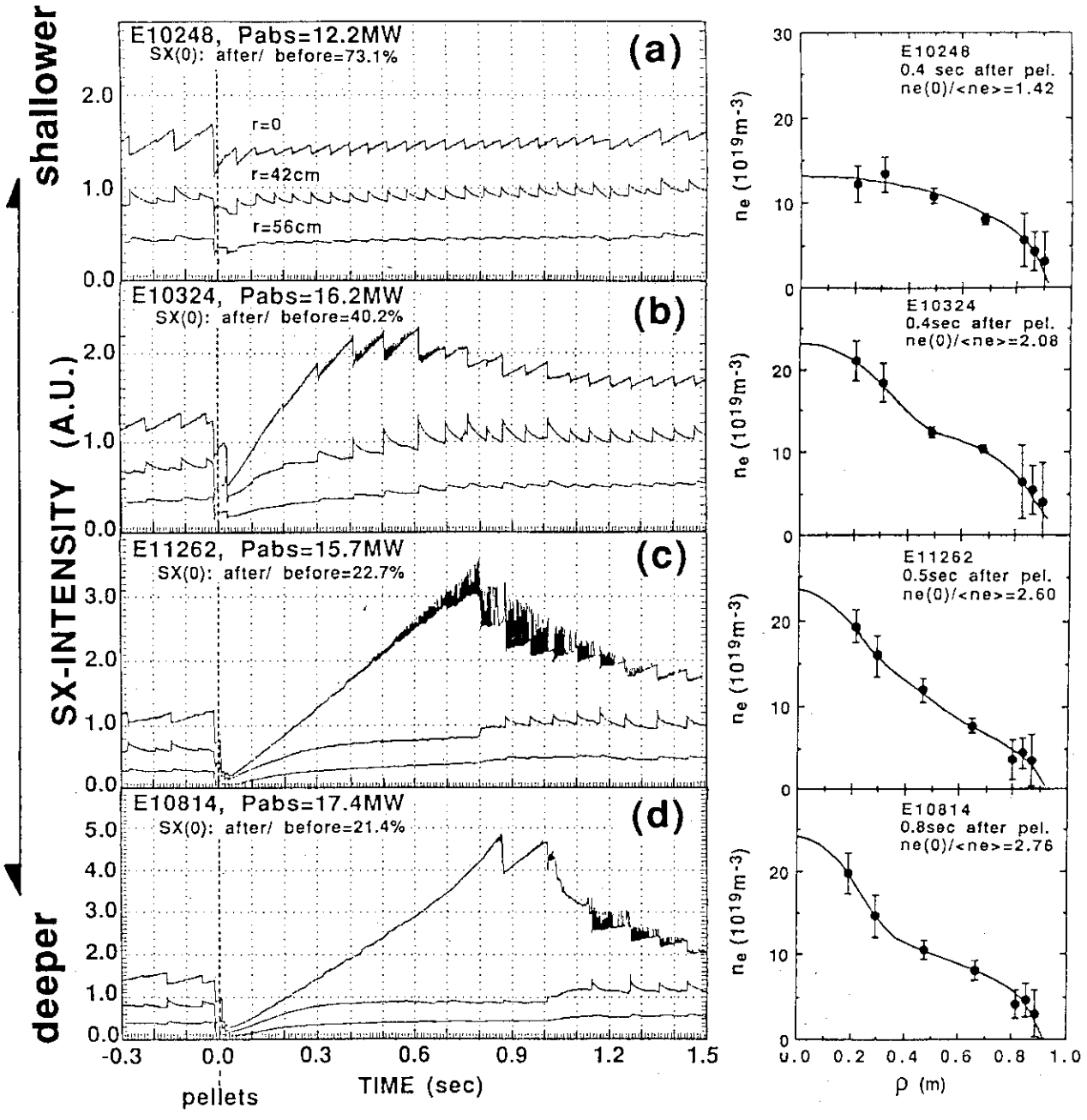

Fig. 18
Time histories of the SX-signals (chords at r=0, r=42 and r=56cm) and the electron density profiles measured with the Thomson scattering system for four pellet injected discharges with q_a~2.3 (Ip=2.8~3.1MA and Bt=4.5~4.8T). The pellet penetration depth becomes deeper from the top (Fig.18(a)) to the bottom (Fig.18(d)) column of the figure.

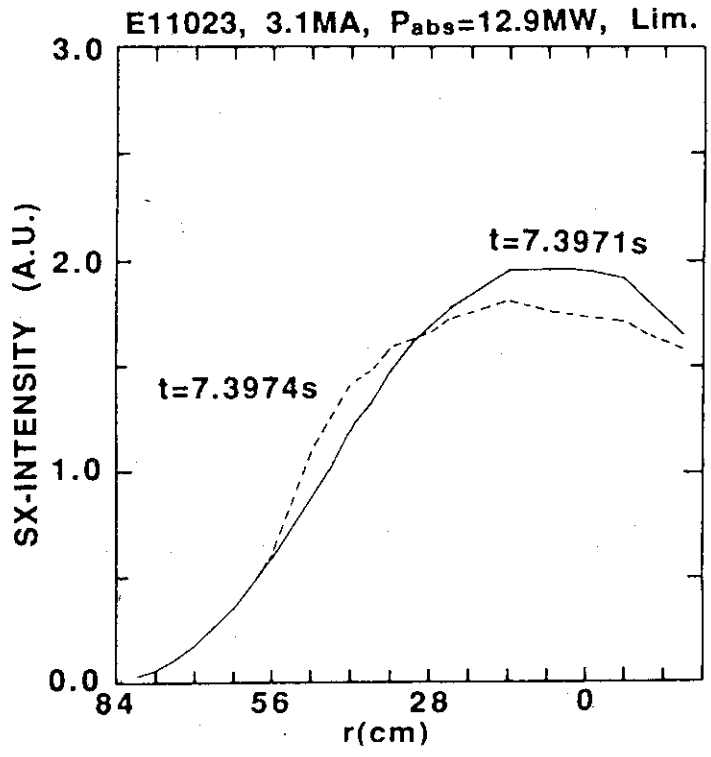

Fig. 19
The SX-profiles just before (t=7.3971s) and after (t=7.3974s) a sawtooth crash are shown for the shallow penetration. In this case, the profile becomes almost flat inside r_s after the sawtooth crash.

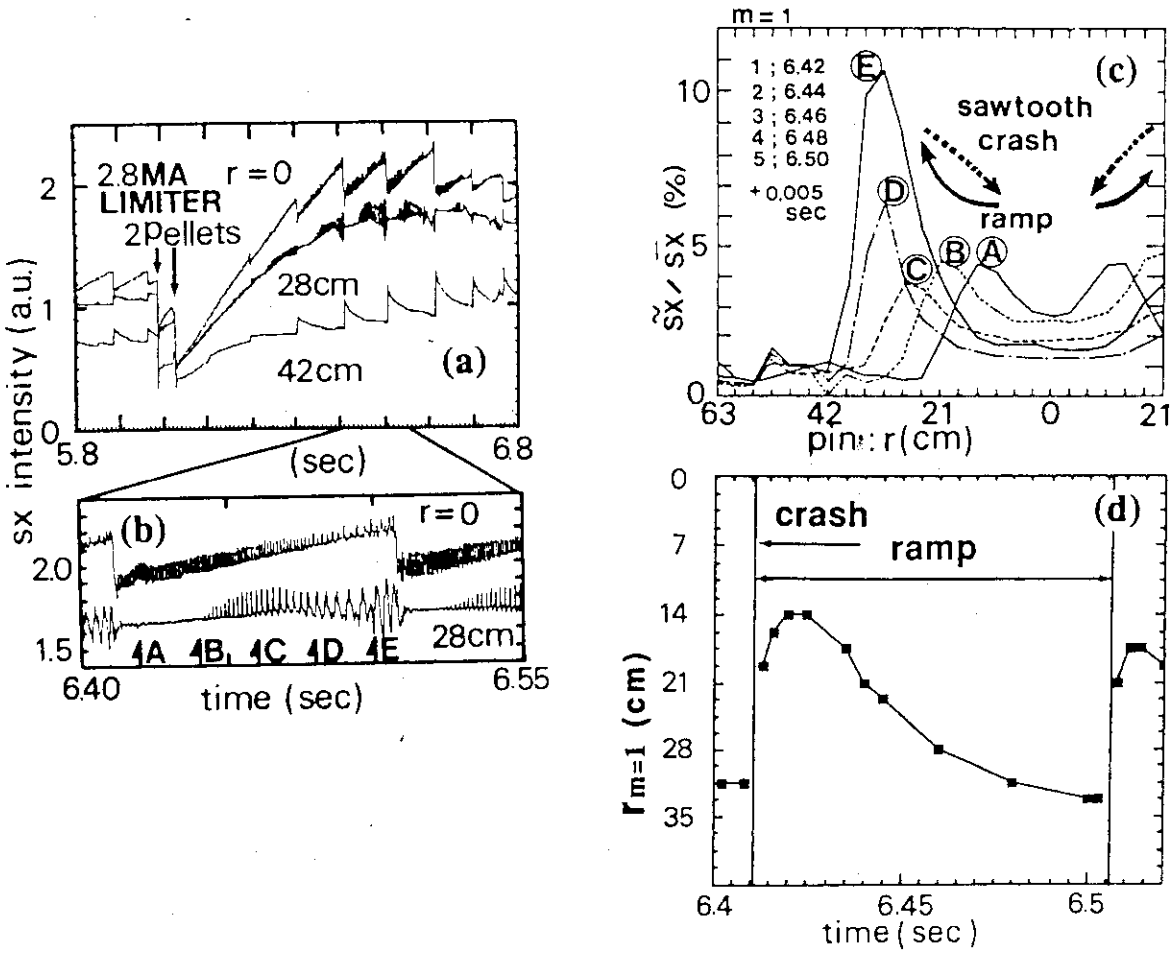

Fig. 20
Behavior of SX emission for the 2.8MA (q(a)=2.34) discharge (E10324; the same discharge with Fig.18(b), the time trace of W^{DIA} was shown in Fig.8.) where the sawtooth activity is not suppressed completely. The high frequency oscillation in (b) is the (m,n)=(1,1) oscillation and the mode appears continuously before (precursor) and after (postcursor) the sawtooth crash. (c) shows the evolution of the profile of $\widetilde{SX}/\overline{SX}$ (fluctuating part/averaged part) for the m=1 oscillation during the sawtooth period. The peak radius of the continuous mode, $r_{m=1}$, is small (~14cm) after the sawtooth crash. The radius increases gradually and reaches 35cm (~a/q(a)) before the next crash. The time evolution of $r_{m=1}$ is given in (d). After the sawtooth crash at t=6.4115sec, $r_{m=1}$ moves inward with the time scale of ~10msec which is much slower than the sawtooth crash time (~400μsec).

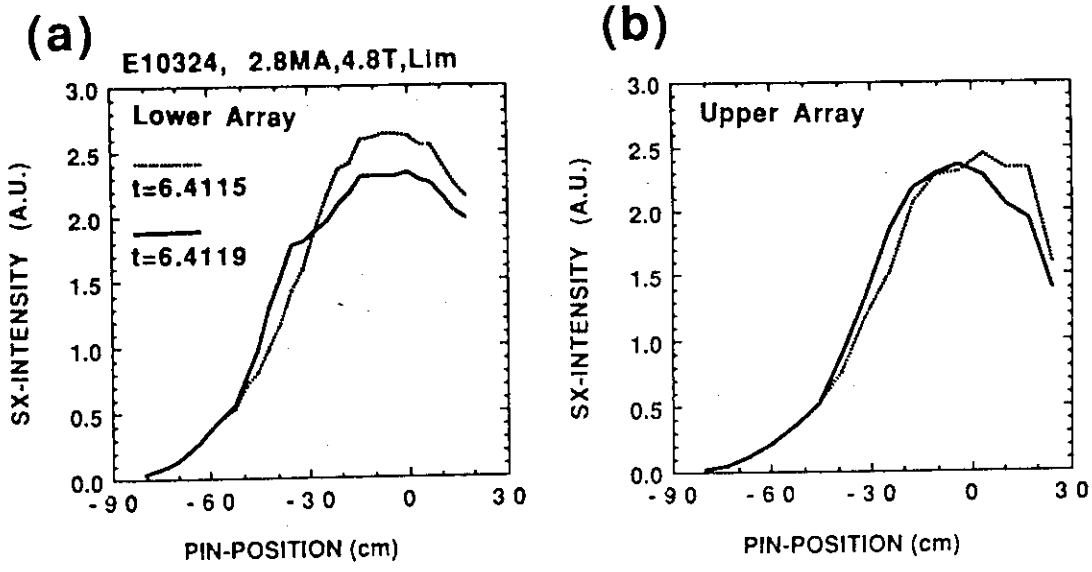

Fig. 21
The SX-emission profiles just before and after the sawtooth at t=6.4115sec. (a) and (b) give the SX-profiles for the lower and upper PIN-diode arrays. The central core shifts (m=1 displacement) and is not flattened completely. (E10324)

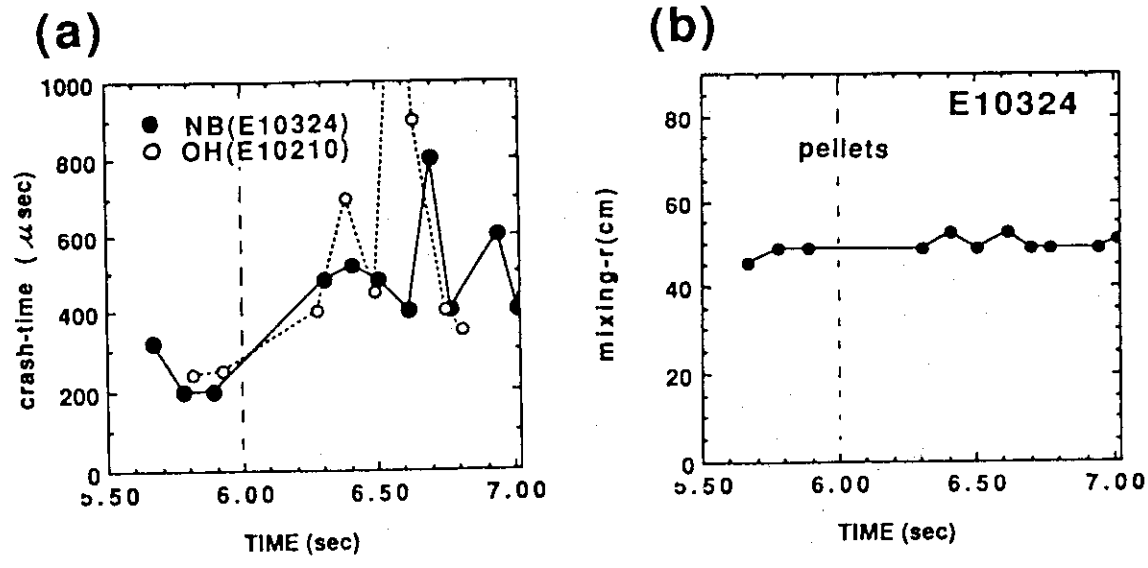

Fig. 22
Time histories of crash times and the mixing radii. After the pellets injected at t=6.0sec, the crash time increases. The sawtooth crash time is typically about 300~600μsec, which is longer than that (~100 ~200 μsec) for gas fuelled discharges. While, the mixing radius dose not change. (E10324)

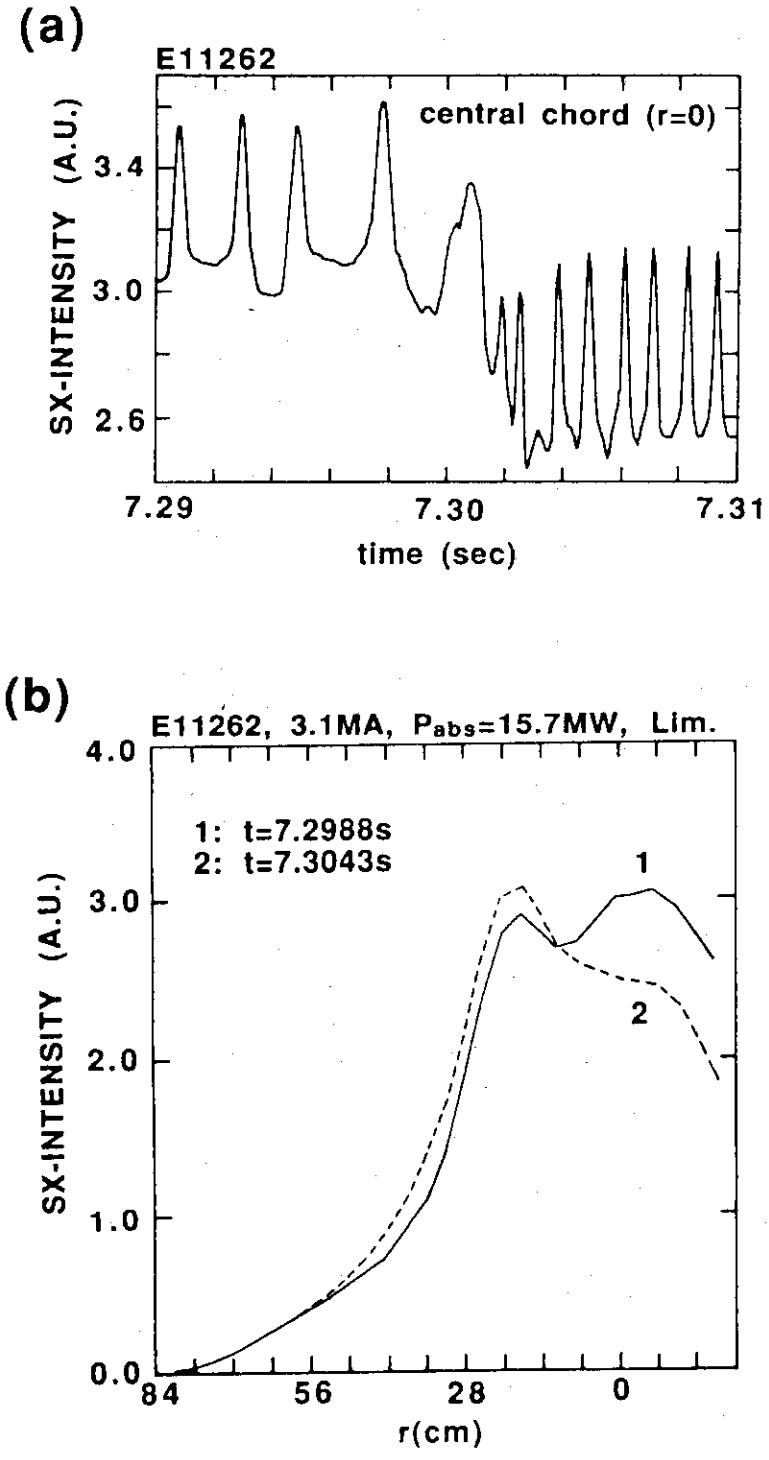

Fig. 23
Time evolution of the central SX-signal and the SX-profiles before and after the sawtooth crash. The timings of t=7.2988s and t=7.3043s are chosen to have the same phase of the m=1 oscillations. Only the central portion of the SX-profile is flattened and the m=1 peak survibes almost unchanged or some amount of the SX-sorce seems to be transported from the central region to the island region. (E11262; See Fig 18(c).)

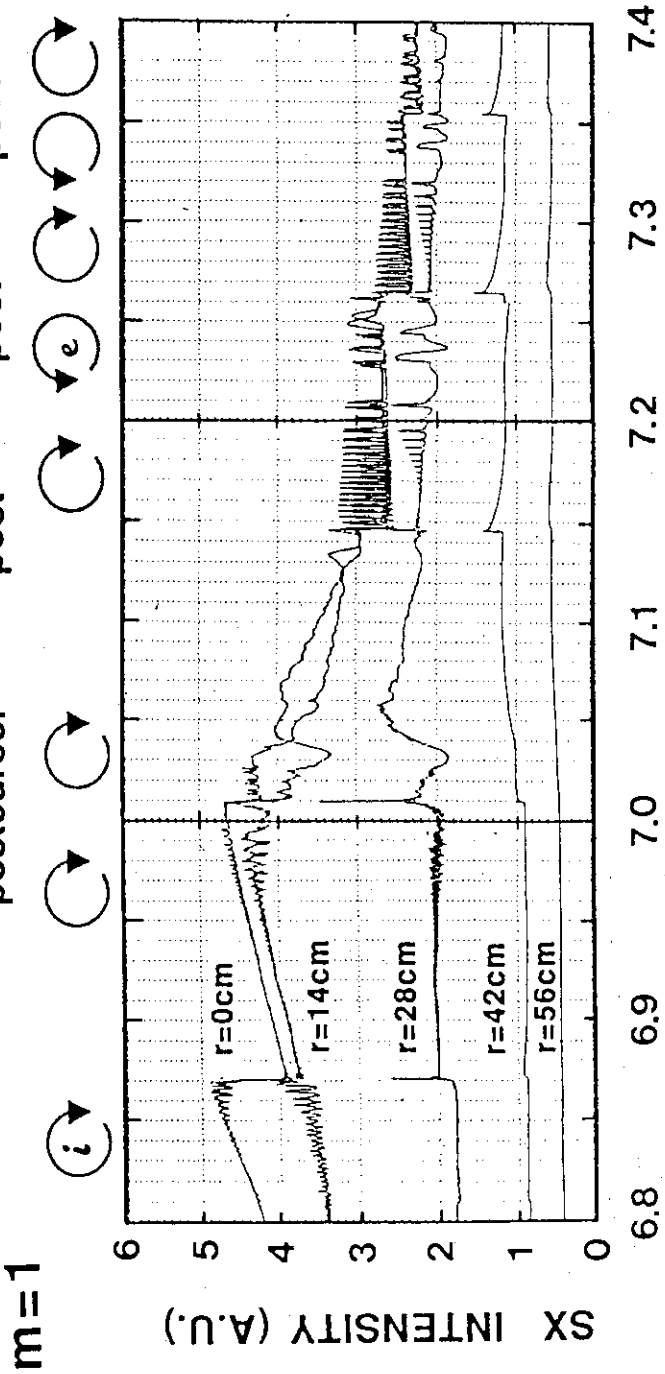

Fig. 24
Time evolutions of SX-signals for E10814 (given in Figs.17 and 18(d)) from t=6.8s to t=7.4s. The first and second sawteeth after the pellet injection (t=6.0s) occur at t~6.87s and t~7.01s, respectively, and the total stored energy dose not decreased due to these sawteeth (see fig.17). (The decrease in W^{DIA} occurs after t=7.03sec.)

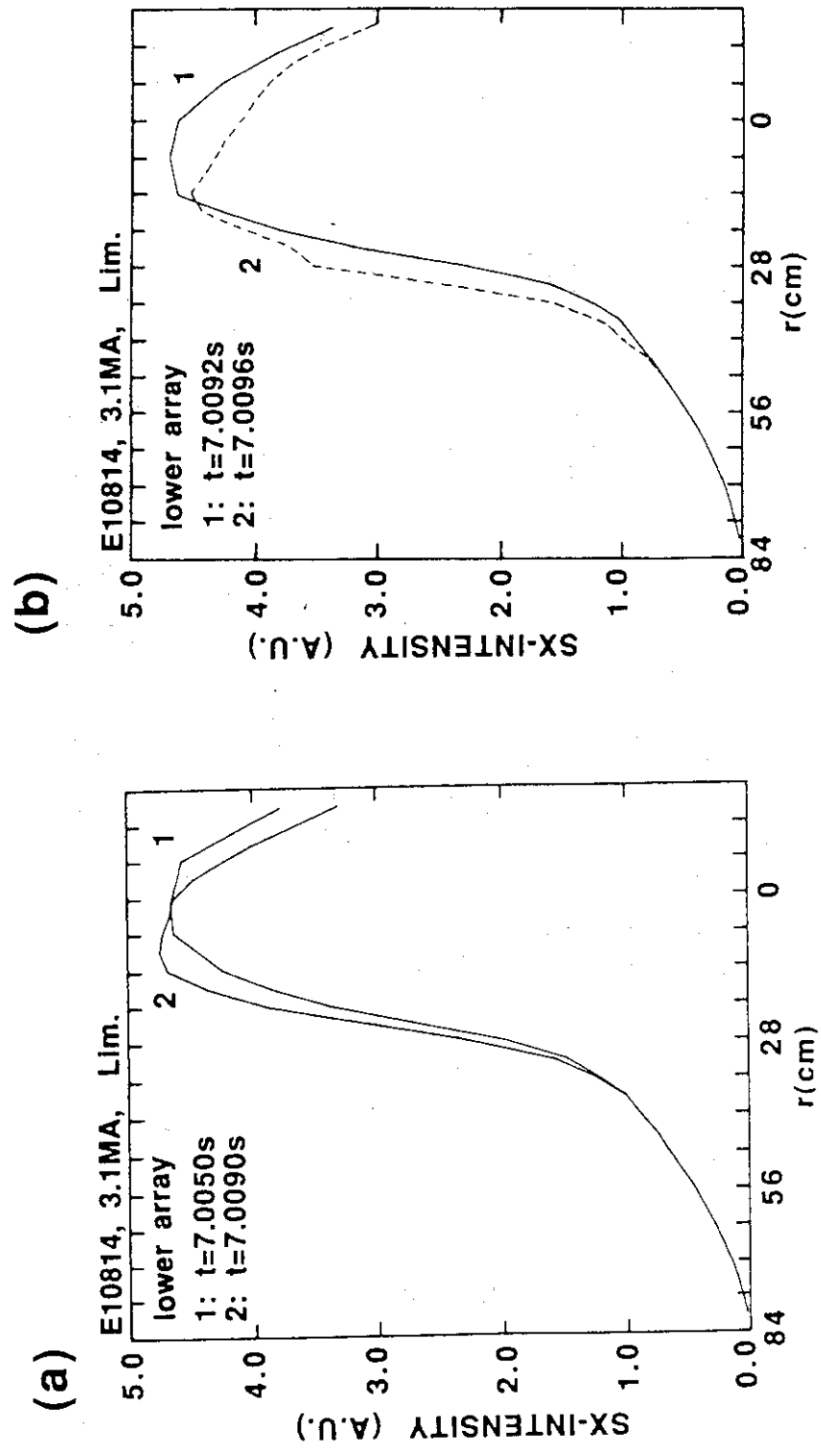

Fig. 25
(a) gives an m=1 shift of the plasma core before the second sawtooth from t=7.005s to 7.009s. With this m=1 displacement, it can be observed that the position of the q=1 surface is at r~35cm. In (b), the change in SX-profile due to the second sawtooth crash is presented. The central core shifts within the crash time of ~400μsec (from t=7.0092 to t=7.0096s), however the almost all of the central sx-source inside the q=1 surface (r<35cm) is conserved and the released energy is small.

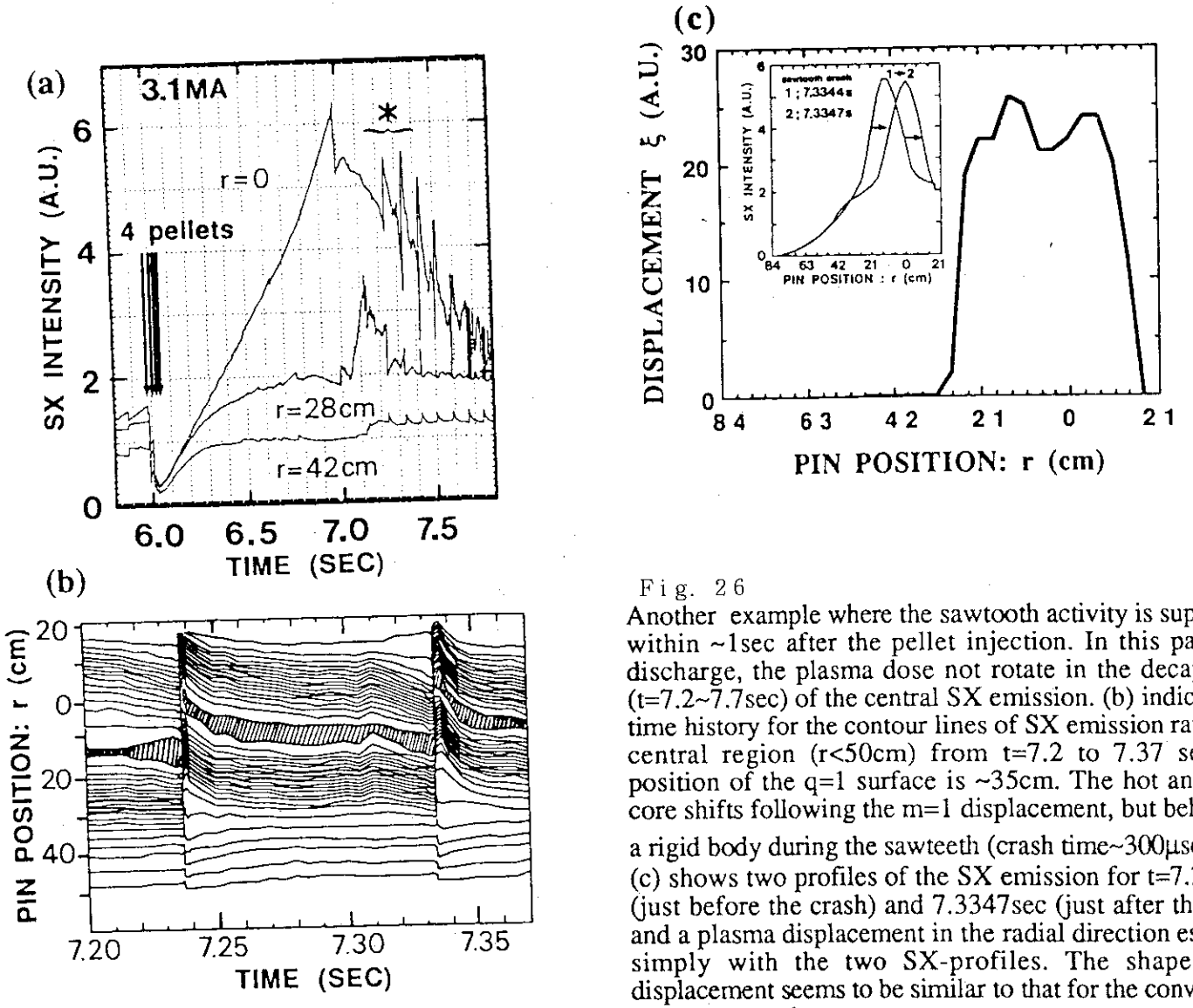

Fig. 26
Another example where the sawtooth activity is suppressed within ~1sec after the pellet injection. In this particular discharge, the plasma dose not rotate in the decay phase (t=7.2~7.7sec) of the central SX emission. (b) indicates the time history for the contour lines of SX emission rate in the central region (r<50cm) from t=7.2 to 7.37 sec. The position of the q=1 surface is ~35cm. The hot and dense core shifts following the m=1 displacement, but behaves as a rigid body during the sawteeth (crash time~300μsec).
(c) shows two profiles of the SX emission for t=7.3344sec (just before the crash) and 7.3347sec (just after the crash) and a plasma displacement in the radial direction estimated simply with the two SX-profiles. The shape of the displacement seems to be similar to that for the conventional ideal m=1 mode.

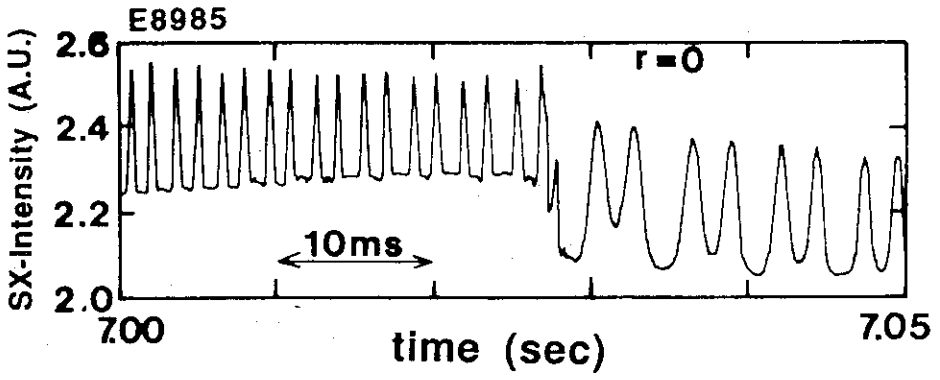

Fig. 27
Time history of m=1 mode before and after the sawtooth for a pellet injected Ip=2.8MA discharge (E8985). In this cases, the m=1 frequency is decreased after the sawtooth crash.

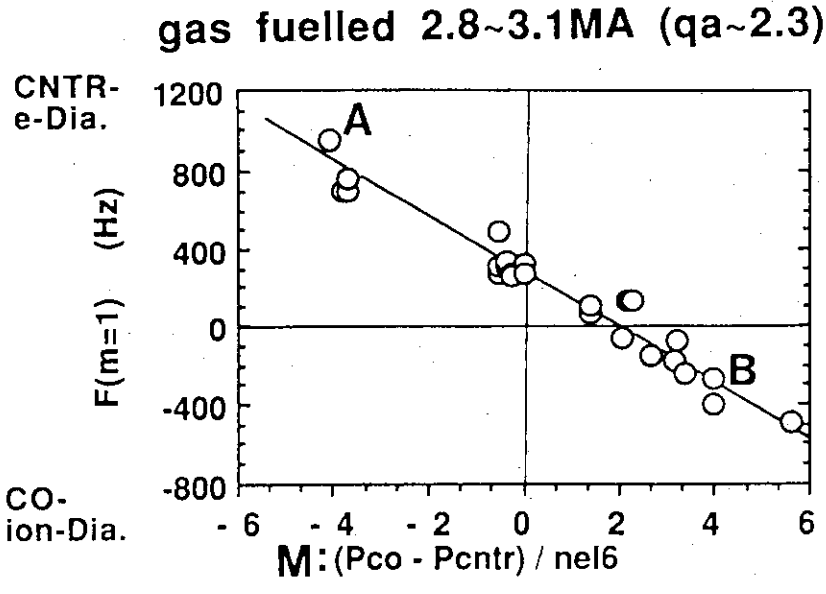

Fig. 28
Relationship between the m=1 mode frequency F and M(=(P_{CO}-P_{cntr}) / n_e) for gas fuelled phase. The positive sign of F corresponds to the counter direction (toroidally) or the electron diamagnetic direction (poloidally). The linear dependence suggests the mode rotates toroidally and F changes with the toroidal momentum input for gas fuelled discharges.

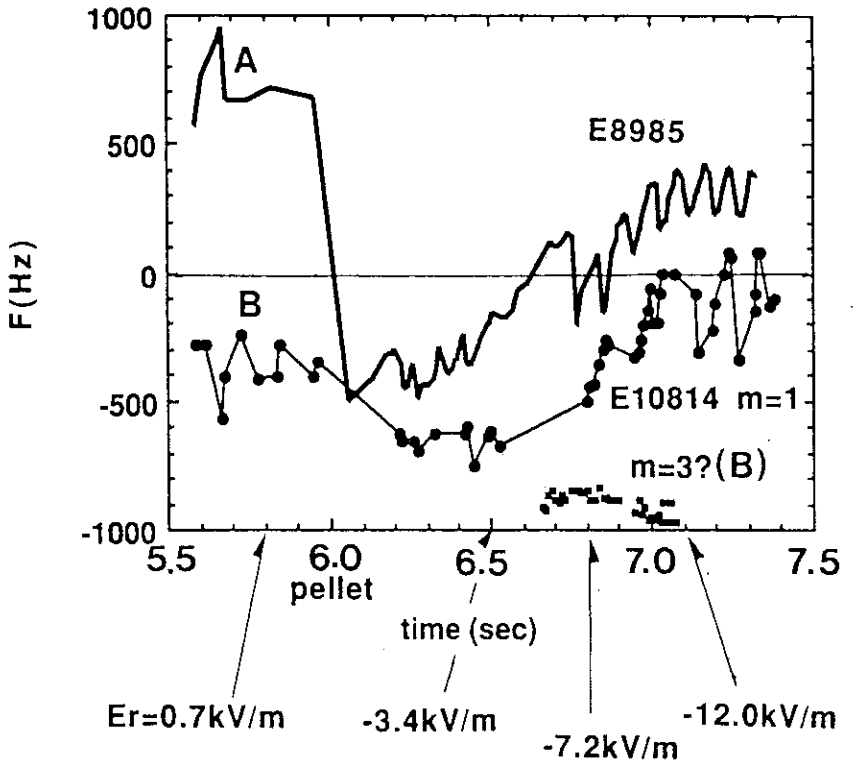

Fig. 29
Time evolutions of F for two discharges A and B shown in Fig. 28. Before the pellet injection (t<0), mode frequencies for A and B have opposit sign. After injection, those for A and B change quickly into negative values (Co- or ion-diamagnetic direction) and, then, recovers gradually to their initial values. First changes in F observed 0.7~1.4 sec after the pellet injection correspond to sawtooth-crashes. The mode frequency crosses F=0 during ramping and crashing phases of sawteeth. Change in the direction of rotation during the sawtooth ramp (t~7.22, 7.33sec) in Fig.24 can be understood as a continuous change in F. Due to the sawtooth-crashes, F changes quickly in the direction of Co- or ion-diamagnetic direction. Time evolution of E_r for case-B (E10814) estimated is alsoindicated.

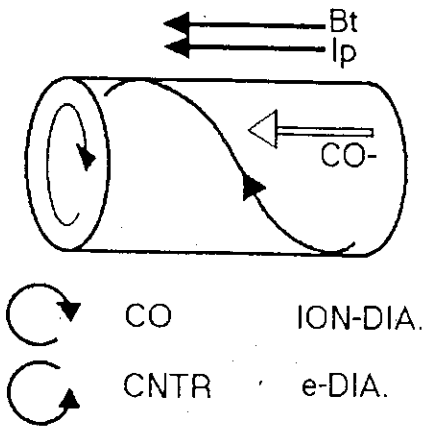

$$E_r=\frac{\nabla Pi}{Zne} - (v\times B)_r$$

$$- v_\theta B_\varphi + v_\varphi B_\theta \quad \text{"}$$

observed freq. ; $F=F\theta+F\varphi$

$Er(v_\theta)=-v_\theta B_\varphi=F_\theta\ 2\pi r_s/m\ B_\varphi$

$Er(v\varphi)= v_\varphi B_\theta=F_\varphi\ 2\pi R/n\ B_\theta$

$(2\pi r_s/m\ B_\varphi)/(2\pi R/n\ B_\theta)=q\,n/m=1$

$Er(v)=(F_\theta+F_\varphi)2\pi r_s/m\ B_\varphi=F\ 2\pi r_s/m\ B_\varphi$

Fig. 30
Schematic drawing of the field line.

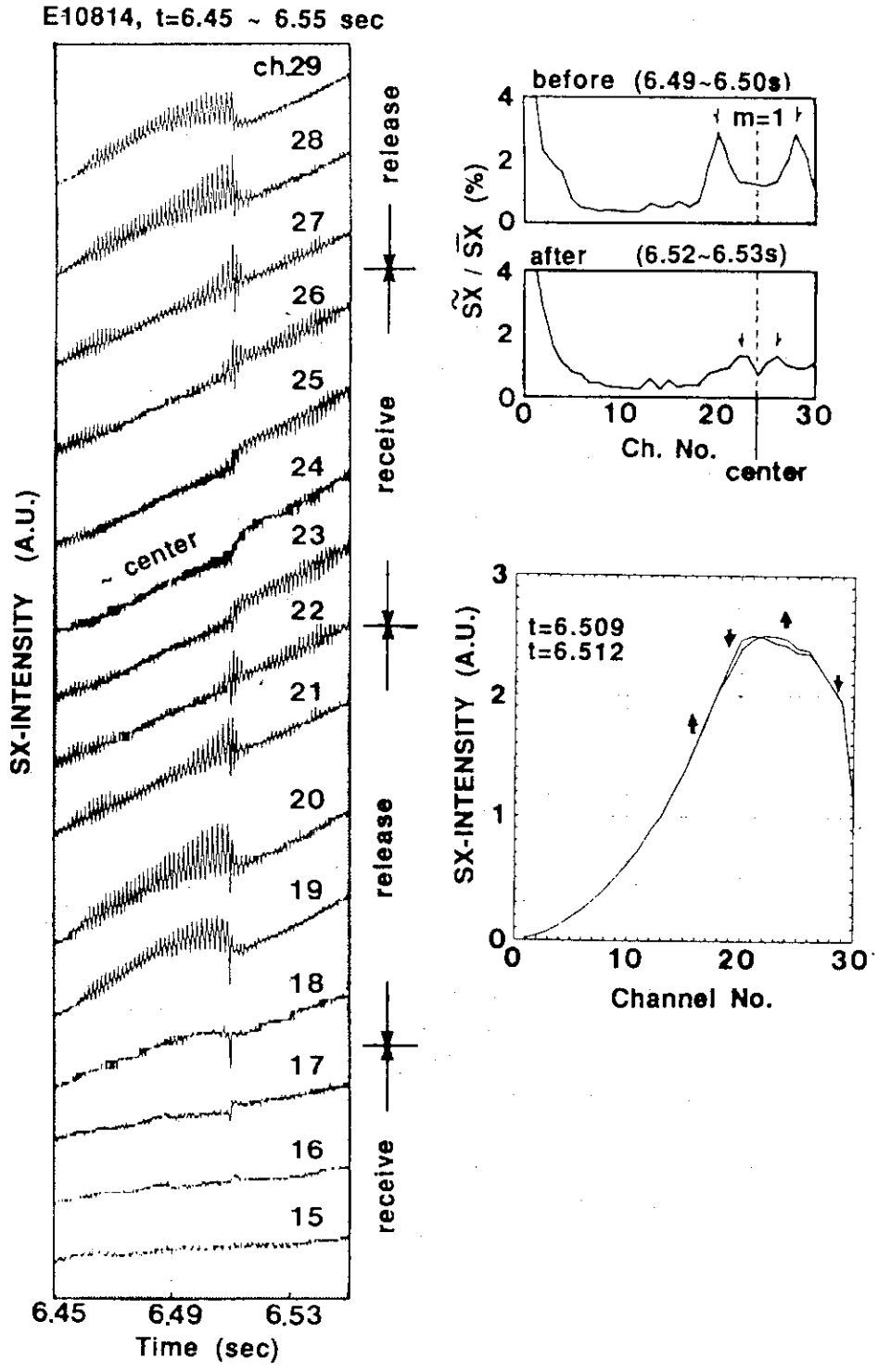

Fig. 31
An example the double sawtooth (E10814). The sawtooth occurs at t~6.51s. After the sawtooth, the SX-intensity for the medium region (chs.21~18 and chs.27~29; 7<r<21cm) releases the energy and that for the central chords (chs.23~25; r<7cm) and the outer region (r>21cm) receive the energy.

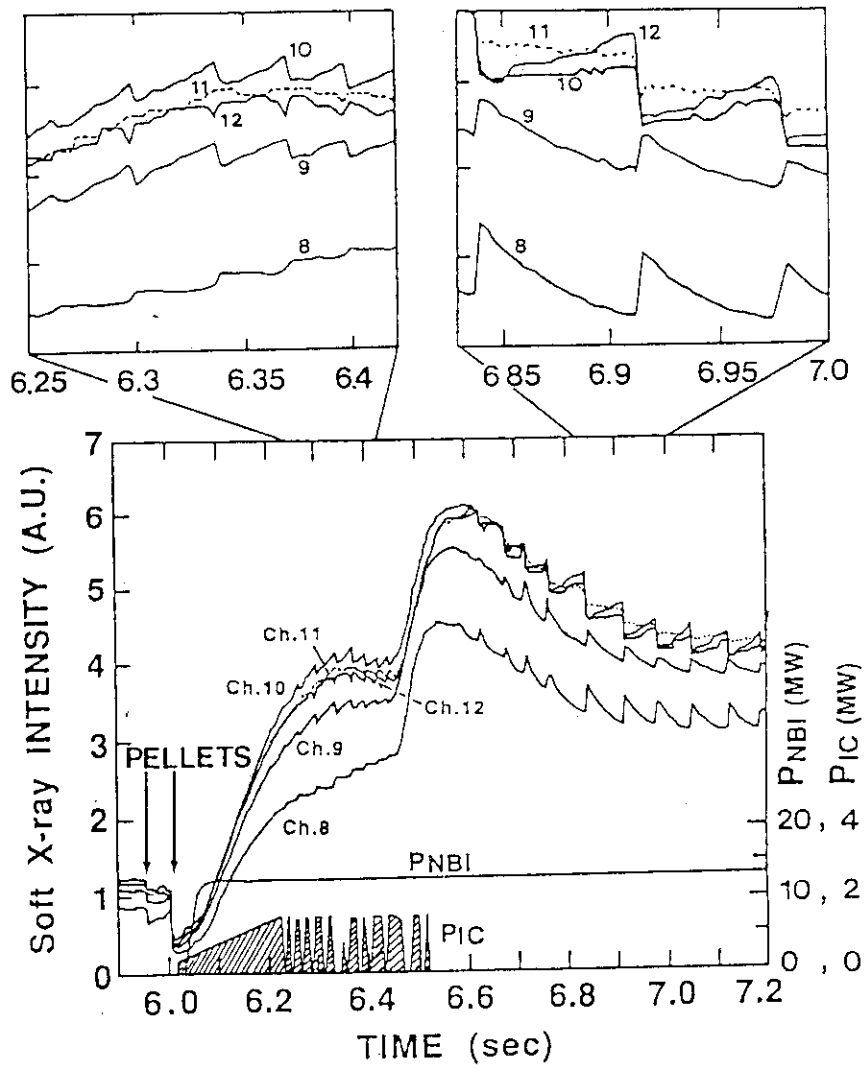

Fig. 32
Double tearing instability is observed during the ICRF heating; the ICRF power was observed to be deposited around ch.9 and ch.10 (r~0.14 ~0.21m) from which the energy was released and the inward and outward heat pulse increases the SX signal at r<0.14m (ch.11,12) and r>0.28m (ch.8). After turn-off of the of-axis ICRF heating, the SX signals happen to increase and show the usual sawteeth oscillations.

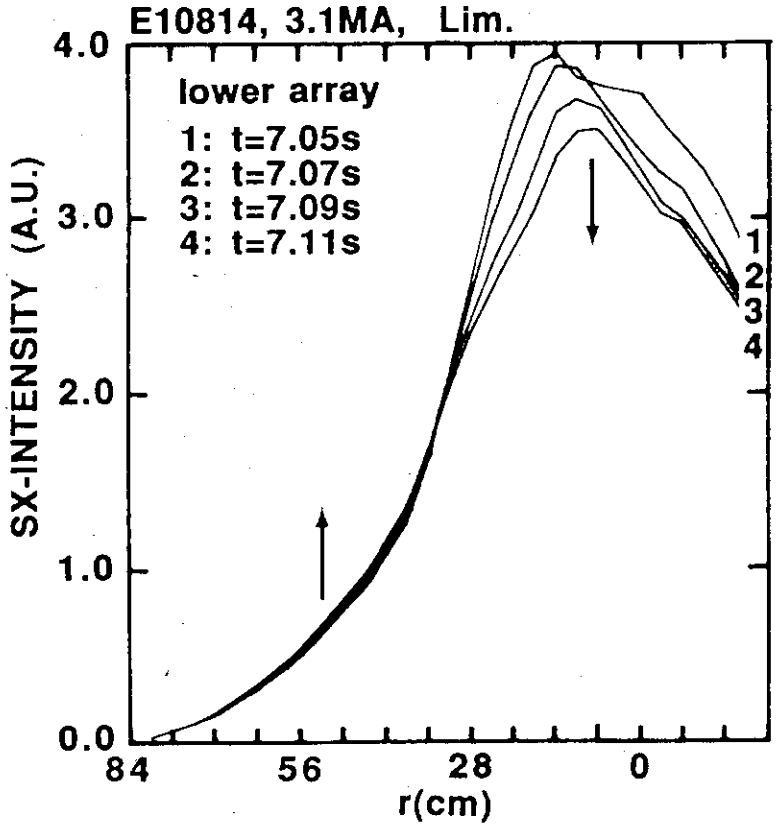

Fig. 33
Time evolutions of SX-profiles for the energy-decreasing phase for E10814 from t=7.05 to 7.11s (see Fig.24). The core seems to be displaced to the left hand side of the figure (t=7.05~7.07s), then the central sx-source is released to the outside the q=1 surface (r~35cm).

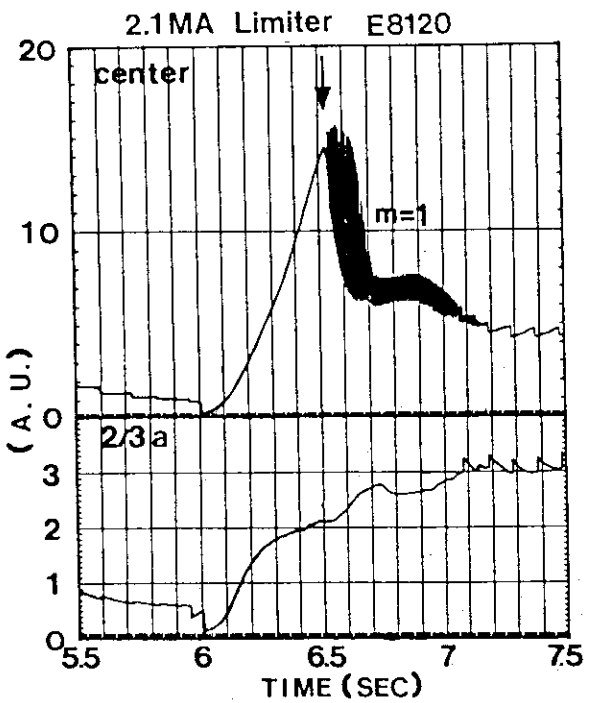

Fig. 34
Another example for the slow release of the central energy. The figure shows the time evolution of the SX-intensity for two chords of r=0 and r~2/3a for a 2.1MA limiter discharge E8120 (the SX-profiles were shown in Fig.5).

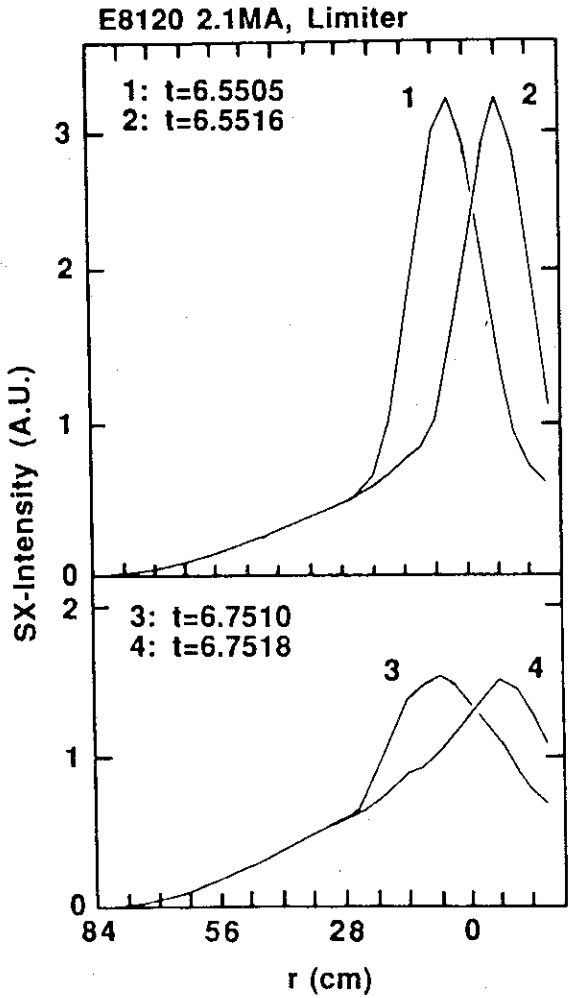

Fig. 35
For E8120 (see Fig.34), the central core happened to be displaced at t~6.53s and a large m=1 oscillation started, then the central sx-intensity decreased slowly. During the decay pase, the spatial distribution of the m=1 character did not change (the figure shows change of the SX-profile due to the continuous m=1 mode around t=6.55s and 6.75s), therefore the slow release is not due to the slow change of the current profile.

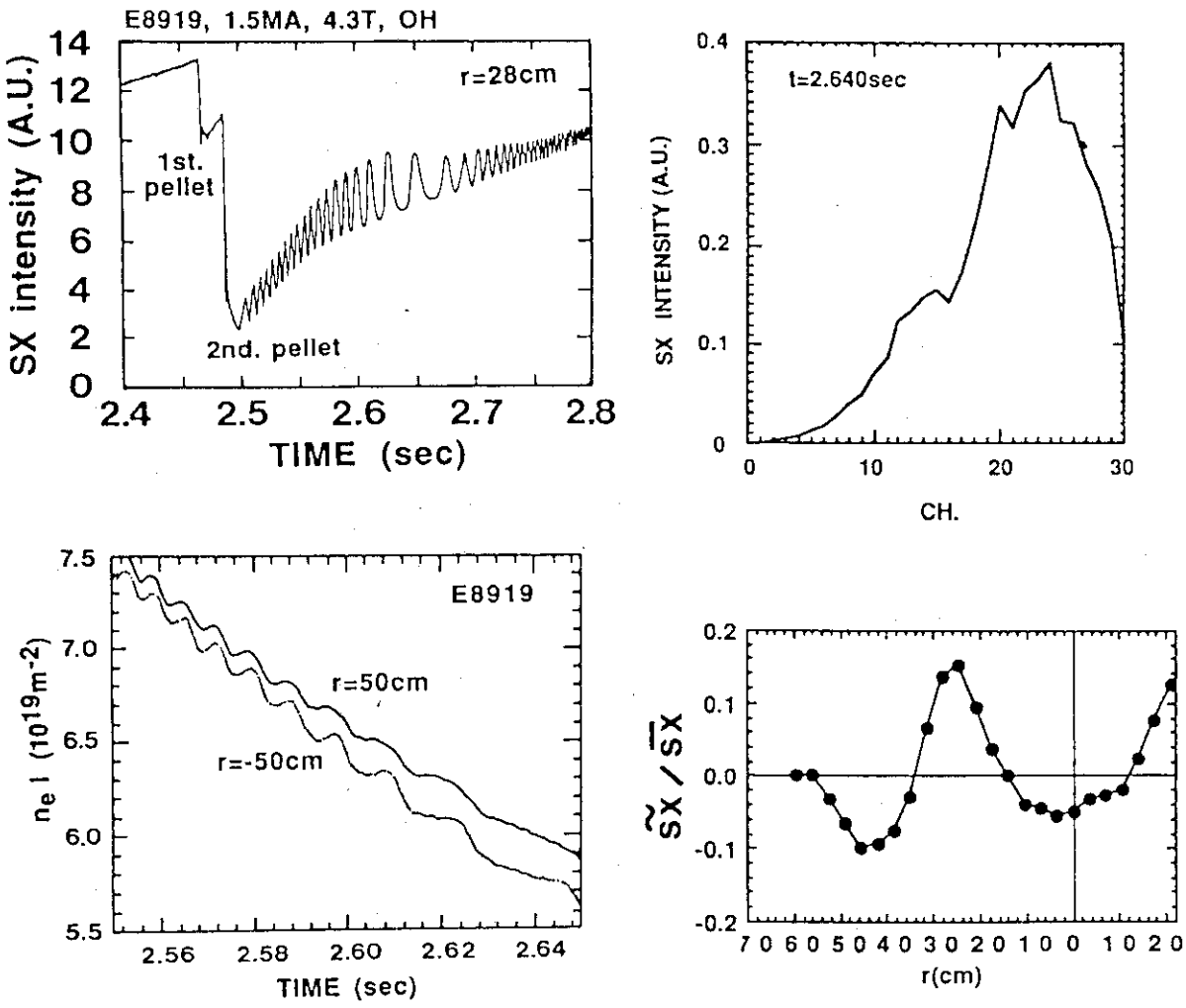

Fig. 36
An example of the m=2 oscillation enhanced by the pellet injection. In this case, pellets were injected just after the ramp-up phase of I_p, therefore, the current profile is relatively flatter than usual target plasma of the pellet injection.A large coherent mode starts just after the second pellet injected at t=2.48sec (see (a)). (b) gives the structure of the mode. Based on the mode pattern, the poloidal mode number of the fluctuation can be identified as a m=2 mode. The spatial distribution of the soft-X ray intensity is shown in (c), where a large amount of the soft-X ray source is observed around ch.9~16 (r=53~28cm). (d) shows time traces of the line integrated electron density measured with two FIR interferometer viewing vertically at r=50 cm and r=-50cm. A large amount of the injected density is trapped inside the m=2 island and the particle confinement is good inside the island.

Appendix A Applicability of SX-signals to estimate the electron pressure

In JT-60 pellet fuelled discharges the SX profile is considered to well reflect that of the electron pressure. Figure A-1(a) compares the profile of square root of Abel inverted soft-X ray intensity and that of the electron pressure n_eT_e measured with the Thomson scattering system for a NB heated 2.1MA limiter discharge. The ordinate for the former is adjusted to have the same value with the latter at r=20cm which is the inner most position measurable with the Thomson system. The soft X ray emission rate is roughly proportional to $n_e^2\ T_e^m$. The SX detection system in JT-60 uses a 250mm thick beryllium window as a SX-filter. For the pellet injected condition on JT-60, Z_{eff}~1.2 and T_e=0.5~2.5keV. If the contribution of heavy impurities for the SX emission rate can be neglected and the main impurity species are oxygen and carbon, m-value is from 1.3 to 2.0 for a parameter regime of Z_{eff}=1.1~2.0 and T_e=0.5~2.5 keV. Therefore, the square root of the SX intensity is in proportion to $n_eT_e^{0.65\sim1}$ which can be considered to give the electron pressure especially for the pellet injected discharges in which the temperature profile is broad and the heavy impurity accumulation is small. Figure A-1(b) shows the comparison between W^{DIA} and the volume integrated SX-intensities for many discharges. Figure A-1(c) also gives the comparison between the time evolutions of these two quantities. These observation shows that the applicability of the SX-intensity to estimate the electron pressure for the pellet fuelled discharges.

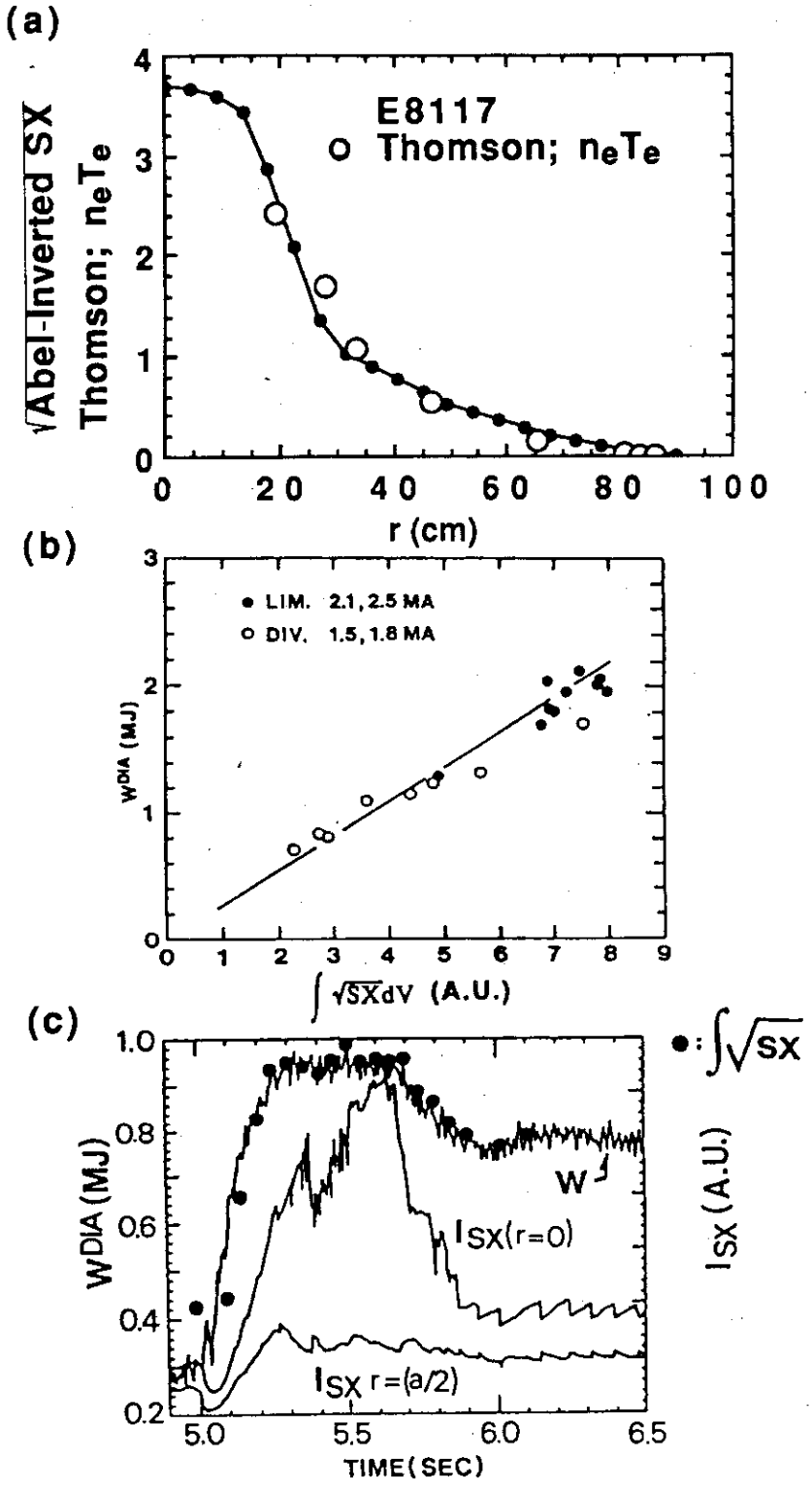

Fig. A－1
(a) compares the profile of square root of Abel inverted soft-X ray intensity and that of the electron pressure n_eT_e measured with the Thomson scattering system for a NB heated 2.1MA limiter discharge. The ordinate for the former is adjusted to have the same value with the latter at r=20cm which is the inner most position measurable with the Thomson system. (b) shows the comparison between W^{DIA} and the volume integrated SX-intensities for many discharges. Figure (c) also gives the comparison between the time evolutions of these two quantities. These observation shows that the applicability of the SX-intensity to estimate the electron pressure for the pellet fuelled discharges.

Appendix B Detailed information of SX-signals for E10814

In this section, the detailed time histories of the discharge E10814 are given. For the global change of W^{DIA}, see Figs. 3 and 17.

Figure B-1 shows the global time evolutions for the SX-intensities. The features of the "double" sawtooth in the early phase after the pellet injection was given in Fig.32.

Figure B-2 gives the time evolutions of the SX-profiles for the upper and lower arrays of the PIN-diode detectors from t=6.1s to t=6.8s. After t=6.4s, the SX-intensity in the outer portion of the plasma (outside ch.14 in the lower figure; r>35cm) is kept almost constant and only that for the central part increases.

Detailed structure of the continuous oscillations (m=1 and m=3?) are given in Figs.B-3 (t=6.8~6.81s) and B-4 (t=6.855~6.865). In Fig.25, time histories of the SX-intensities were given from t=6.8 to 7.4s.

The precursor m=1 oscillations and additional oscillation (m=3?) before the first sawtooth after the pellet injection are shown in Fig.B-5 (t=6.85~6.88). The interesting features of the figure is that i) the m=3? oscillation (typically shown for chs.18~14) is kept almost unchanged even after the sawtooth crash and ii) a large spike of the sx-intensity is observed to start at the end of the sawtooth crash for the outer channels. The latter observation suggests that the central core, once displaced strongly at the main portion of the sawtooth crash, recovered to the cylindrical profile.

The evolution of the SX-profiles around the sawtooth are given in Figs.B-6(a) and (b). Those during the crash phase are given in (a) at t=6.8700s, 6.8705s and 6.8706s. The core is displaced to the left direction in the figure.With the initial displacement of the core, the position of the q=1 surface is around r~31~35cm. At t=6.8708s (Fig.B-6(b)), the core started to move the opposite direction and the peak of the profile reaches r=0cm at t=6.8713s. What is interesting is that the released amount of the central SX-source inside the q=1 surface is very small.

The evolutions of the SX-profiles around the second sawtooth was given if Fig.26.

The stored energy starts to decrease after t~7.03sec. The time scale for the release of the central energy is very long compared to the sawtooth crash time (see Fig.34).

Figure B-7 shows rotating features of the m=1 mode from t=7.1463 to 7.1495s. From the shape of the rotating peaks, the SX-source seems to be confined in an island with a crescent profile.

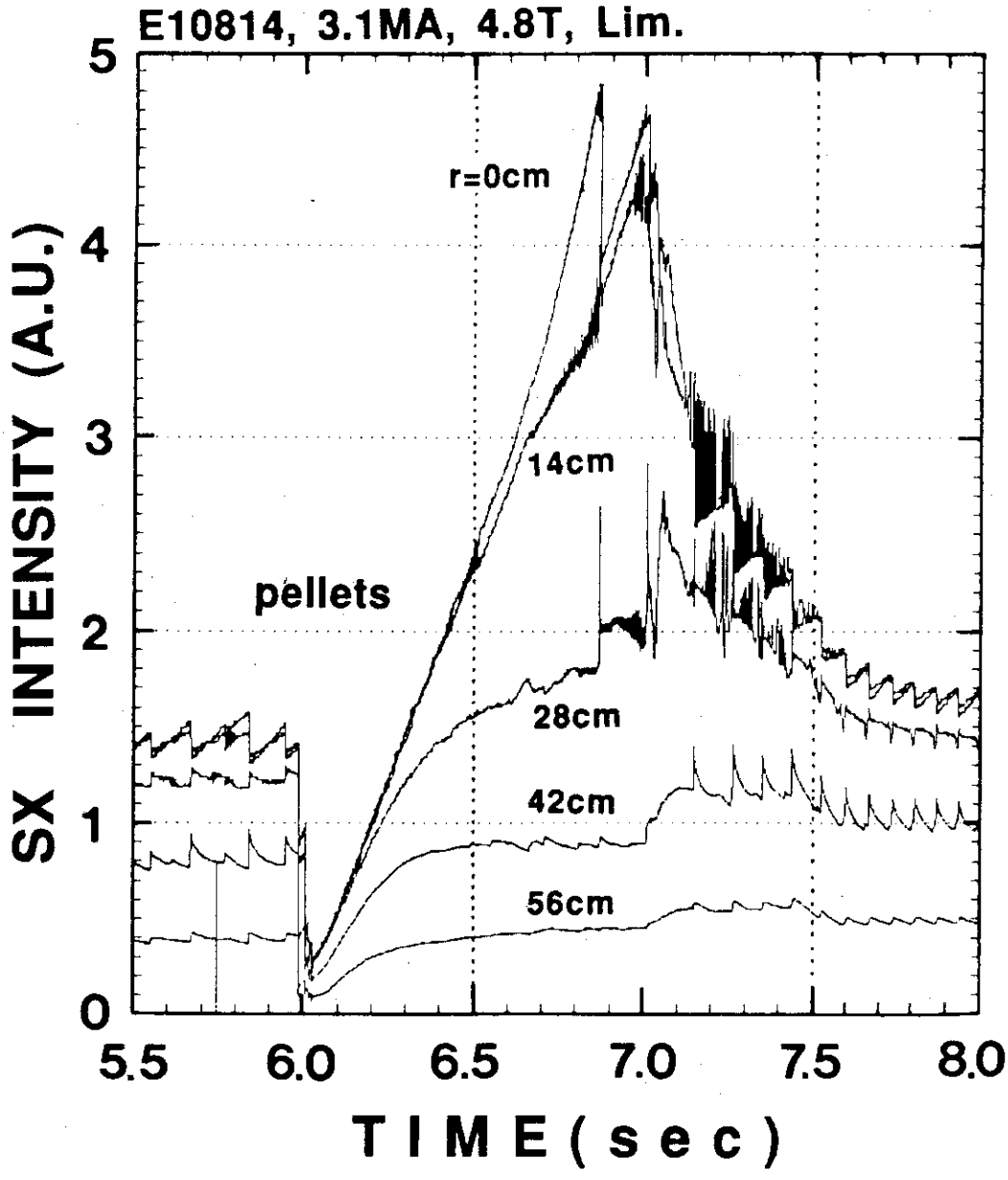

Fig. B-1
Global time evolutions for the SX-intensities.

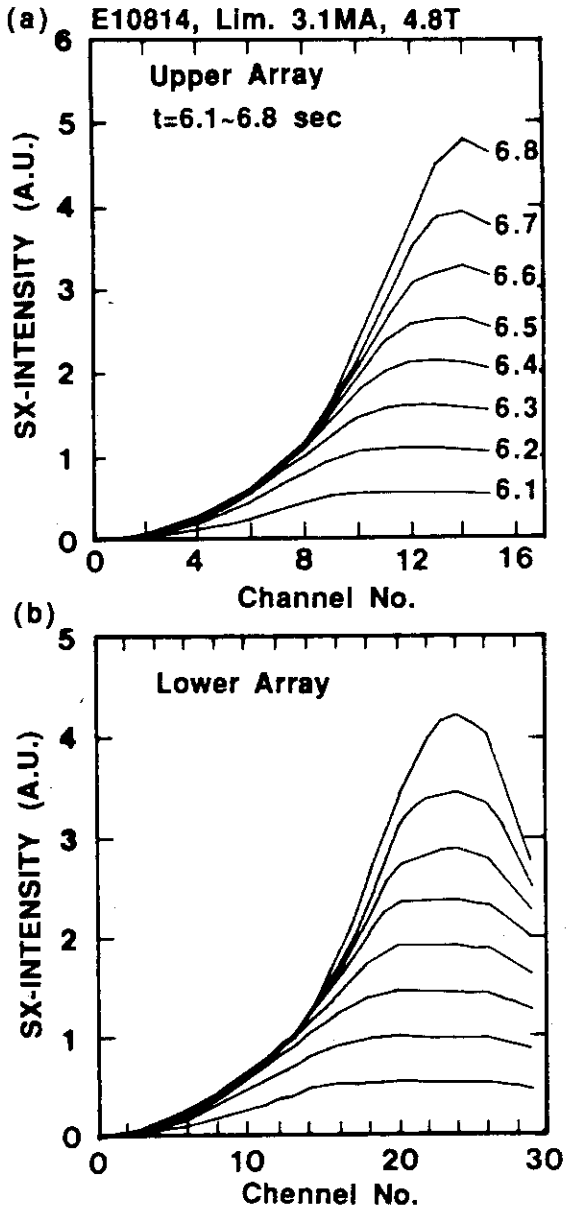

Fig. B-2
Time evolutions of the SX-profiles for the upper and lower arrays of the PIN-diode detectors from t=6.1s to t=6.8s. After t=6.4s, the SX-intensity in the outer portion of the plasma (outside ch.14 in the lower figure; r>35cm) is kept almost constant and only that for the central part increases.

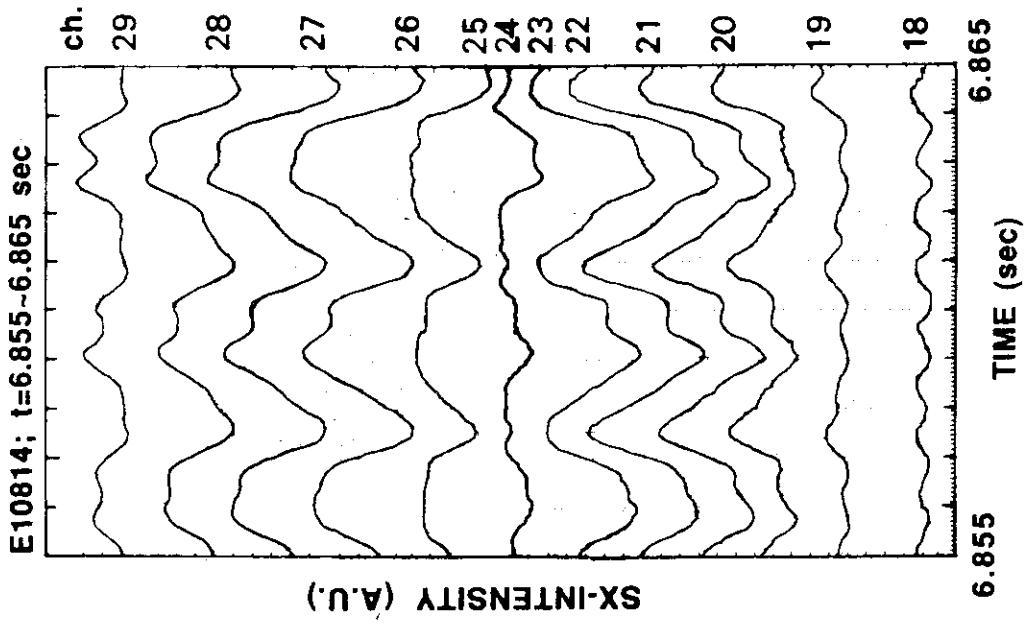

Fig. B-4
Time histories of the continuous oscillations from t=6.855s to 6.865s.

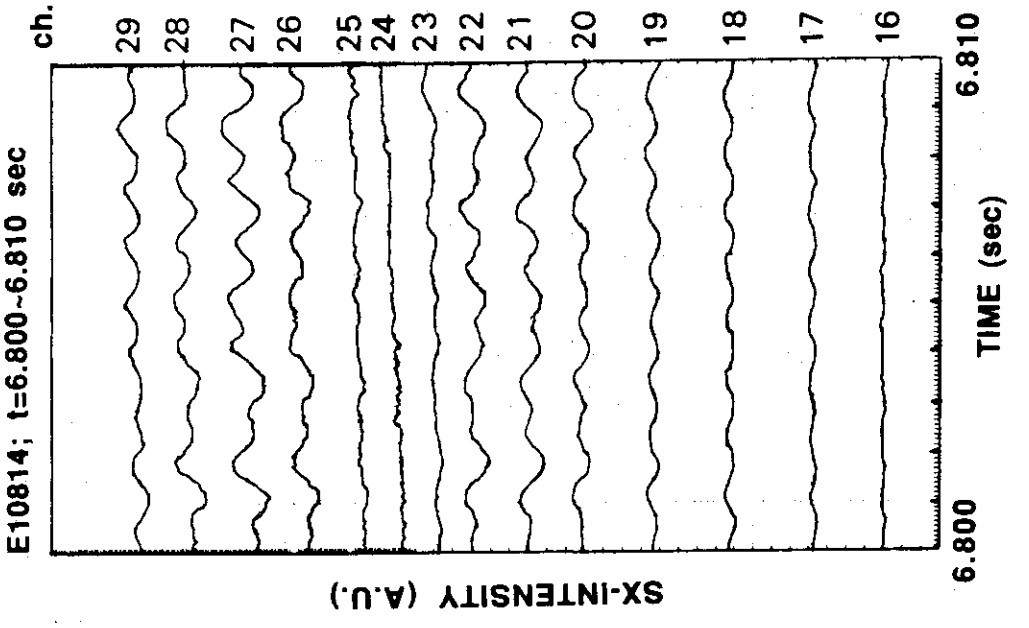

Fig. B-3
Time histories of the continuous oscillations from t=6.80s to 6.81s.

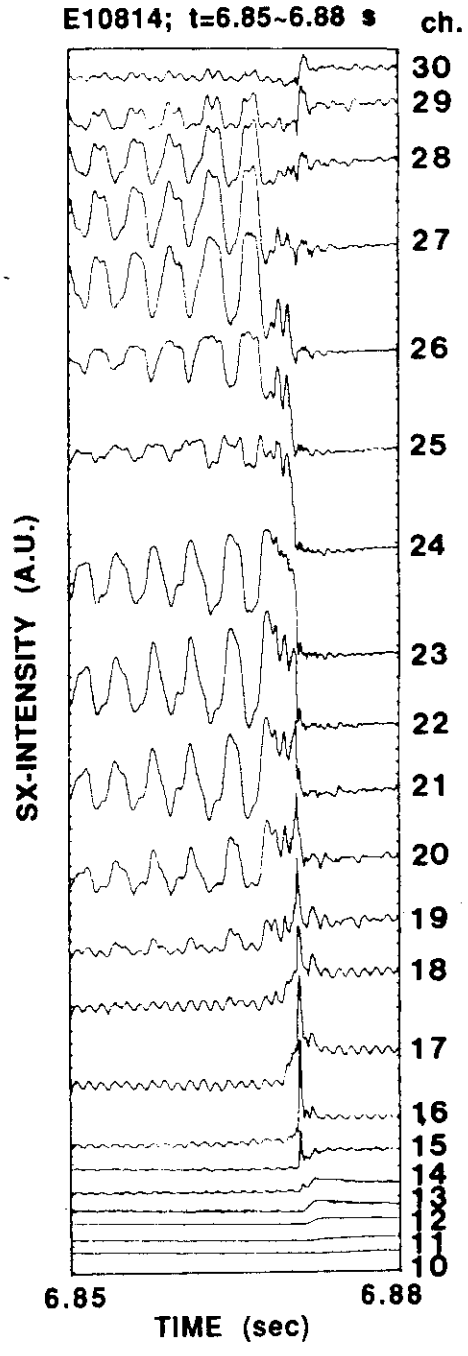

Fig. B-5
The precursor m=1 oscillations and additional oscillation (m=3?) before the first sawtooth after the pellet injection. The interesting features of the figure is that i) the m=3? oscillation (typically shown for chs.18~14) is kept almost unchanged even after the sawtooth crash and ii) a large spike of the sx-intensity is observed to start at the end of the sawtooth crash for the outer channels. The latter observation suggests that the central core, once displaced strongly at the main portion of the sawtooth crash, rocovered to the cylindrical profile.

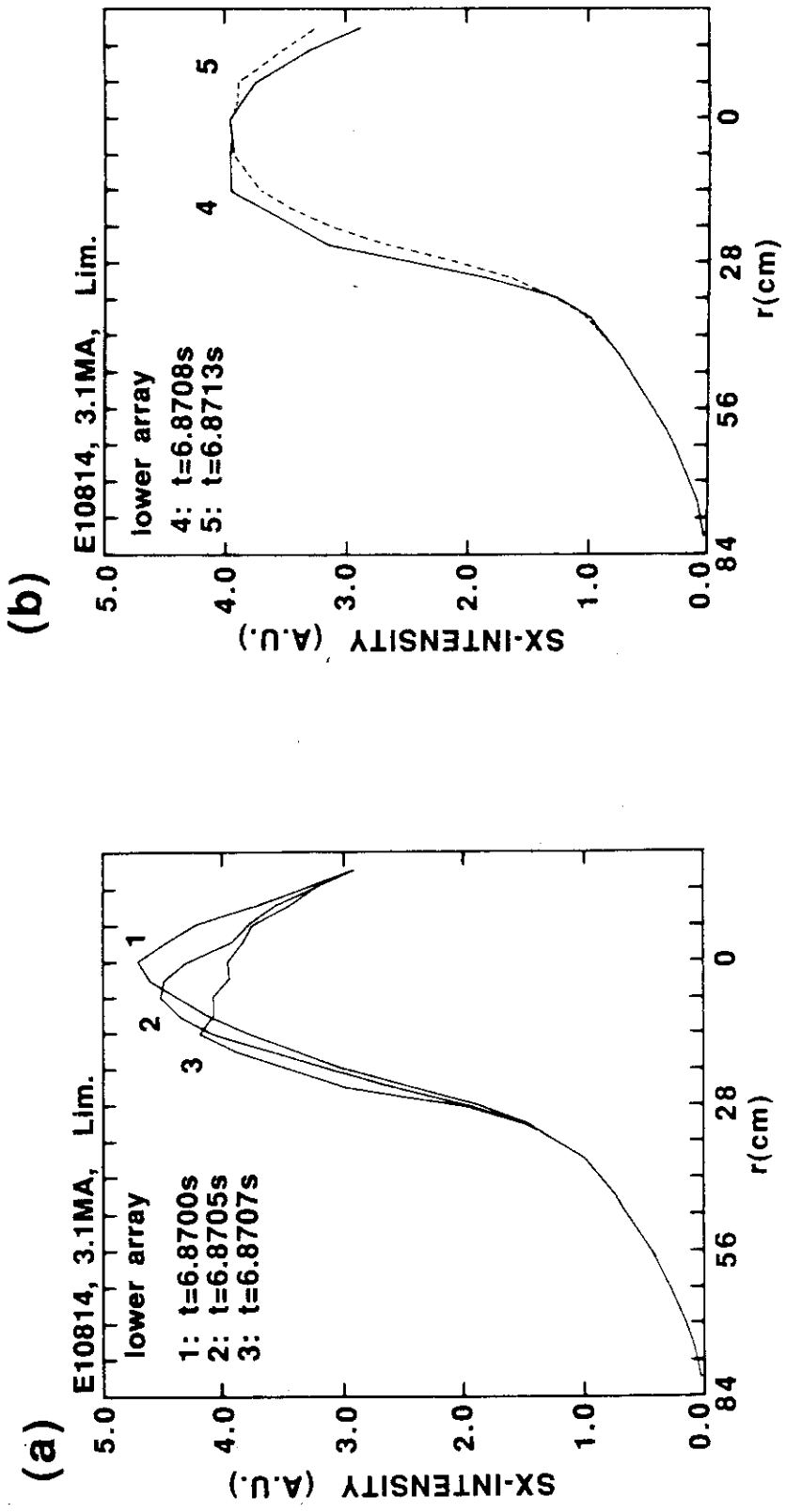

Fig. B－6
The evolution of the SX-profiles around the first sawtooth. Profiles during the crash phase are given in (a) at t=6.8700s, 6.8705s and 6.8706s. The core is displaced to the left direction in the figure. With the initial displacement of the core, the position of the q=1 surface is around r~31~35cm. At t=6.8708s ((b)), the core started to move the opposit direction and the peak of the profile reaches r=0cm at t=6.8713s. What is interesting is that the released amount of the central SX-source inside the q=1 surface is very small.

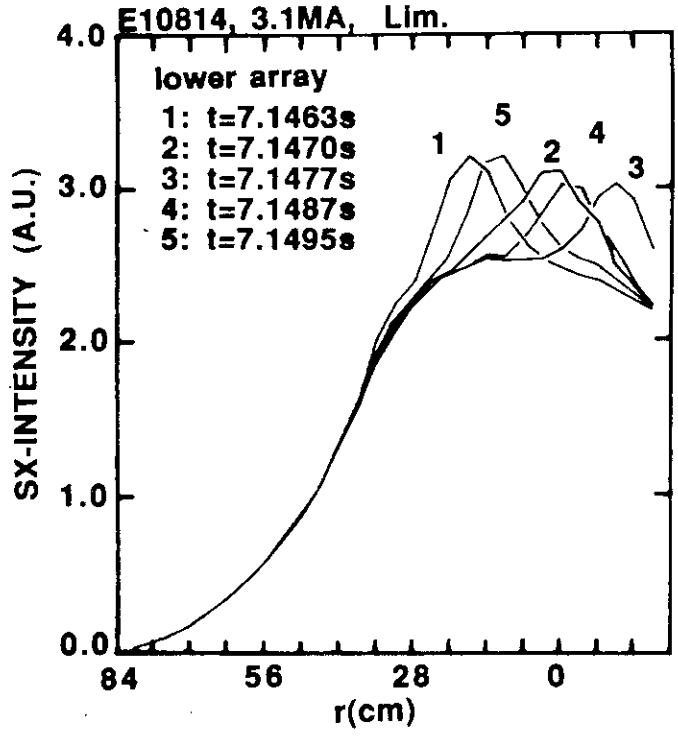

Fig. B－7
Rotating features of the m=1 mode from t=7.1463 to 7.1495s. From the shape of the rotaing peaks, the SX-source seems to be confined in an island with a crescent profile.